Paper 71

Synthesis, Characterization and in Silico Prediction of Oxime and Thiosemicarbazone Derivatives of Halo Hydroxy Naphthoquinone As An Anti-Viral Agent Against SARS2 Corona Virus

Raju Murkute[a] and Sanjay Gaikwad[b*]

a Deccan Education Society's Fergusson College (Autonomous), Shivaji Nagar ,Pune

b Bharatiya Jain Sanghatana's Arts, Science commerce College, Wagholi, Pune

Abstract:

Oxime and thiosemicarbazide derivatives of halo juglone synthesized for antiviral activity. Characterization of juglone derivatives are done by IR and NMR Spectroscopy. RM1 –RM6 molecules are selected for in silico study. National Centre for Biotechnology Information server found proteninase (PDB id:2ALV) was found SARS corona virus for serve acute respiratory syndrome. 3 D X-ray crystallographic structure of proteinase (PDB id:2ALV) which was validated on Ramchandran Plot was 99.2% by using PROCHEK server. Auto dock Tools version 1.5.6 was used to optimize 3D module of protein. X-Ray crystal structure as three dimensional coordinate of these target protein was obtained from the research collaborator for structural Bioinformatics (RCSB) protein data bank. Binding pockets has been verified by using PDB sum server. Autocad tools was used for receptor grid calculation. Docked conformation of ligands with 2ALV obtained from Maestro V12.8. Possible ligand binding site in the minimized protein were determined by Computed Atlas of Surface Topography of proteins (CASTp) server. For docking studies, we used the AutoDock Vina 1.1.1, with 1 ˚A of spacing between the grid points. The PASS server provides all the possible activities of the given halohydroxynapthaqunone derivatives. Final result was analysed by pymol and lig plot indicate that RM2, RM3 and RM6 showing better activities towards proteinase (PDB id 2ALV) of SARS2.

Kyewords : Juglone, Oxime and thiosemicarbazide derivatives, Corona Virus, Silico Prediction

Introduction:

All world experienced covid-19 major outbreak .Coronavirus disease (Covid -19) is an infectious diseases caused by SARS- Cov-2 virus. The corona virus is affecting 221countries in the world, and 237,155,841 people infected all over the world. 4,842,331 death occurs till death due to covid -19 all over the world. There is no successive clinical trial for covid-19. [1]

Ayurveda is great gift for India which is curative and preventive. Juglone which is present in the bark, roots and leaves of Julandiace family has been used traditionally in ayurvedic medicine for the treatment of anti-inflammatory, antioxidant, antimicrobial, anti-viral and antitumor activities. [2-5]

In pharmacological processes binding of protein with drug is important parameter. Bonding between drug molecule and protein is based on binding energies. Bonding angles, hydrogen bonding, π interactions,Van der Waals interactions are also affecting parameter for bonding between drug molecule and protein. Metabolism between drug molecule and protein impact on

therapeutic effects of drug, interaction of drug molecule to protein effects on stereo –chemical changes of proteins. [6]

In silico predication is the first step in drug development. On the basis of literature survey oxime and thiosemicarbazide derivatives of halo-juglone molecular docking have not been reported.

Activity spectra predication done using PASS online module, by way 2 drug server. For the docking study protein was isolated from RCSB online data base. Protein and ligands optimization was done by various software Grid parameter obtained from Cast p server. Actual docking was done using autodoc tools 4.2.

Discovery studio lig plot and maestro used for analysis of protein- ligand complexes. We found that RM2 ,RM3 shows better affinity with the receptor.

Experimental:

Preparation of 2 Chloro Juglone:

Dichloro Juglone derivatives was refluxed in 20 cc ethanol using water bath for 2 hrs after attaining 80 C temperature . The solution was dried in vaccum .The compound containing a mixture of 2 – chlorojuglone and dichlorides. This is tested by TLC using solvent (9:1 n-hexane : ethyl acetate). The product 2-Chloro Juglone purified by column chromatography using silica gel 200 mesh size and 9:1 n -hexane + ethyl acetate mixture as elute. The melting point was 164 C.% yield obtained 42 %.

IR (cm^{-1}):744, 785, 844,909, 1049, 1088, 1193, 1297, 1448, 1587, 1637, 3051,. C^{13}NMR:187.311, 181.245, 144.775, 140.96, 134.62, 133.28, 132.211, 131.643, 125.456, 120.629., ^{1}H NMR(δ):7.94 (s,1H), 7.87 (d,1H), 7.80 (ddd,1H), 7.69 (d,1H) , 2.47(s,1H)

Preparation of 2- Bromo Juglone:

5.00 g of Juglone suspended in 50 ml of glacial acetic acid containing 1.5 ml of bromine was shaken mechanically for 15 minutes. The solution which soon took place was poured with stirring into much cold water. The dibromide separated as a reddish Yellow mass of crystal which is melted at 102ºC.The dibromide it was then dissolved in 15 cc of absolute alcohol and heated under reflux condenser for 45 minutes. 6.1 g of monobromoJuglone crystallized in reddish brown plates, the pure product with melting point of 164ºC. % yield obtained 36%.

IR (cm^{-1}):737.57, 871.46, 1129.1, 11199.32, 1245.65, 1580.89, 1639.37, 3060.05., C^{13}NMR:187.494, 181.641, 144.211, 140.283, 135.931, 135.231, 130.691, 127.89, 125.453, 120.999., ^{1}H NMR(δ):7.81 (s,1H), 7.67 (d,1H), 7.53 (ddd,1H), 8.69 (s,1H) , 2.30(s,1H)

Preparation of 2 Iodo Juglone:

The diiodo product is refluxed in 20 ml ethanol using oil bath for 2 hr after maintaining temperature of 80ºC. The solution was dried in vacuum .The compound containing a mixture of 2–iodo juglone and diiodide. This is tested by TLC using solvent (9:1 n-hexane : ethyl acetate). The product 2-iodo Juglone purified by column chromatography using silica gel 200 mesh size and 9:1 n -hexane + ethyl acetate mixture as elute. The melting point was 168ºC, yield obtained 55%.

IR (cm^{-1}) :745.45, 832.78, 857.56, 1097.86, 1157.50, 1277.97, 1491.11, 1593.44, 1633.68, 2920.07., C^{13}NMR:190.100, 183.869, 146.76, 139.813, 136.613, 131.610, 124.542, 120.544, 114.240., ^{1}H NMR(δ):8.50 (d,1H), 7.87 (ddd,1H), 7.33 (d,1H), 8.57 (s,1H), 2.30(S,1H)

Preparation of 2- bromojuglone mono-oxime (RM1), 2- Iodojuglone mono-oxime (RM2), 2-chloro-juglone mono-oxime (RM3)

0.3 g (2-bromo, 2-iodo, 2-chloro derivative of juglone) dissolved in 10 ml 1 M NaOH solution and 0.1043 g hydroxylamine hydrochloride in 5 ml distilled water. Solution is kept in water bath for 1 hour at 50ºC. Then let it cool to room temperature. Solution is then diluted with ice cold water to 50 ml. Add 1Molar HCl to adjust the pH to 5.5. Then solution is kept in ice bath for 2 hours and allowed to precipitate. Precipitate is filtered through Whatmann filter paper and dried completely. Procedure for removal of acid by solvent separation method is carried out, yield obtained 63%, 65% and 54% respectively. [7-12]

RM1: IR (cm^{-1}): 3362, 3155, 1630, 1576, 1293, 1211, 1050, 784, 740,676., C^{13}NMR:182.26, 166.678, 161.275, 147.213, 133.756, 133.0, 132.621, 122.634, 121.802, 120.3., ^{1}H NMR(δ):7.4 (d,1H), 7.87 (dd,1H), 7.60 (d,1H), 7.29 (S,1H) , 5.31 (S,1H), 8.47(S,1H)

RM2: C^{13}NMR:183.231, 164.693, 162.371, 147.689, 133.987, 132.774, 123.659, 122.731, 121.956, 100.853,. ^{1}H NMR(δ):7.32(d ,1H), 7.57 (dd,1H), 7.42(d, 1H), 8.29 (S, 1H) , 5.41 (S,1H), 2.67(S,1H)

RM3: IR (cm^{-1}):3341, 3140, 1654, 1545, 1320, 1234, 1065, 952,770, 660., C^{13}NMR:182.313, 166.916, 161.646, 138.790, 133.543, 133.869, 131.537, 124.834, 122.642, 122.93., ^{1}H NMR(δ):7.82 (d,1H), 7.54 (dd,1H), 7.12 (d,1H), 7.29 (S,1H) , 5.62 (S,1H), 2.37(S,1H)

Preparation of semicarbazide derivatives of 2-bromo Juglone (RM4), 2-iodo Juglone (RM5), and 2-chloro Juglone (RM5)

2 mol of methanolic solution of (2-bromo, 2-iodo, 2-chloro derivative of juglone) is added to 10 ml of 0.2 N NaOH to obtain reddish brown purple solution. 0.02 mol of 50 % methanolic solution of thiosemicarbazone is added drop wise with constant stirring for 3 hours. The solution is neutralized using 10% HCl till precipitation. Then the solution is filtered and recrystallized in methanol. Melting point135ºC, yield obtained 67%, 70% and 63% respectively. [13-18]

RM4: IR (cm^{-1}):3373, 3270, 3255, 1684, 1620, 1535, 1270, 1023, 778, 654, 590,. C^{13}NMR:187.342, 182.881, 165.483, 160.221, 148.195, 133.892, 132.672, 131.324, 129.953, 125.678, 123.692., ^{1}H NMR(δ): 7.72 (s,1H), 7.64 (d,1H), 7.52 (d,1H), 7.29 (dd,1H), 3.12 (s,1H), 5.34 (s,1H) 2.37(S,2H)

RM5: IR (cm^{-1}):3356, 3290, 3276, 1679, 1530, 1276, 980, 875, 679, 543., C^{13}NMR:187.342, 184.881, 165.483, 163.221, 146.195, 137.892, 135.672, 133.212, 124.512, 100.2,. ^{1}H NMR(δ):8.72 (d,1H), 7.64 (dd,1H),7.59 (d,1H),7.39 (s,1H) ,4.12 (s,1H),5.34 (S,1H) 2.37(S,2H)

RM5: IR (cm^{-1}):3300, 3265, 1720, 1656, 1578, 1323, 987, 890, 766, 593,. C^{13}NMR:188.312, 186.631, 166.439, 165.384, 155.613, 145.542, 130.617, 131.781, 135.212, 127.684, 121.319,. ^{1}H NMR(δ):7.67(d,1H), 7.44 (dd,1H), 7.31 (d,1H), 7.19 (1H), 4.11 (s,1H), 5.49 (s,1H), 2.35(s,2H)

Methodology:

Selection of particular Ligands from monooxonaphthalenone derivatives

The important derivatives from synthesized compounds were used in the present investigation for the computational prediction of potential drugs from it by the process of molecular docking against Covi-19.

Biological Activity Prediction

Due to the impossibility of performing a study of the biological activity of a large number of compounds in a short period, it was decided to conduct a preliminary assessment of the potential biological activity of compounds (RM1, RM2, RM3, RM4, RM5 & RM6) using PASS-online modeling. The PASS software product, which predicts more than 300 pharmacological effects and biochemical mechanisms on the basis of the structural formula of a substance, may be efficiently used to find new targets (mechanisms) for some ligands and, conversely, to reveal new ligands for some biological targets. The mean accuracy of prediction with PASS is about 86% in LOO cross-validation. The tool uses the descriptors to predict the activity of a substance. [19-22]

Result:

The prediction of the biological activity spectrum of oxonaphthalenone derivatives RM1 to RM6 revealed that compounds are determined as promising SARS coronavirus main proteinase. This indicates that all the three compounds may show good activity against Covid-19 as SARS coronavirus main proteinase is main target for covid treatment.

The 3D SDF structures of the processed six halo hydroxyiminonaphthalenone derivatives RM1 to RM6 were given as an input for PASS server. The PASS server provides all the possible activities of the given halo hydroxyiminonaphthalenone derivatives as promising SARS coronavirus main proteinase inhibitors. PASS can be effectively applied to predict biological potential of compounds and to analyze large chemical databases. PASS predicted search results show all the available information on the pharmacological and toxicological activity of all the three compounds analysed. Similar observation in accordance with the present study using PASS server was already reported by many researchers. Pa and Pi are the estimates of probability to be active and inactive respectively from the biological activity spectrum. Their values vary from zero to one. Each active compound possesses a number of biological activities. Its specificity of action is always relative and is defined by the peculiarities of object, dose, route, etc. Biological activity spectrum of compound can be predicted on the basis of structure-activity relationships found by the analysis of the known data from the training set. Based on the analysis of large training set consisting of tens of thousands of the known biologically active compounds, computer program PASS provides the means to evaluate any new compound in huge chemical-pharmacological space. On the basis of this study it can be reveals that all the three compounds may show good activity against Covid-19 as SARS coronavirus main proteinase inhibitor.

Molecular Docking Studies:

Target Protein Retrieval and Preparation

On the basis of literature survey we found that SARS coronavirus main proteinase is major target to study anti-covid study. Therefore, fasta sequence of SARS coronavirus main proteinase

for Severe acute respiratory syndrome-related coronavirus was retrieved from National centre for biotechnology information server and done Basic Local Alignment Search for regions of similarity between biological sequences available on Protein Data Bank. Then Three-dimensional X-Ray crystallographic structure of SARS coronavirus main protease (PDB id: 2ALV) was obtained from PDB databank which was validated using various parameters like resolution, Mutation and Ramachandran plot.[23-25] Details are as follows.

Table1. Comparison between standard values and retrieved protein for validation of protein selected for docking study

Parameters	**Details**	**Standards**
Protein Id and method of experiment	2ALV X-RAY Diffraction	- X-RAY Diffraction
Mutation	No	No
Resolution	1.90 A^0	Near about 2.00 A^0
Ramchandran Plot (by PROCHECK server) Residues in favoured + Allowed regions	99.2 %	>88 %

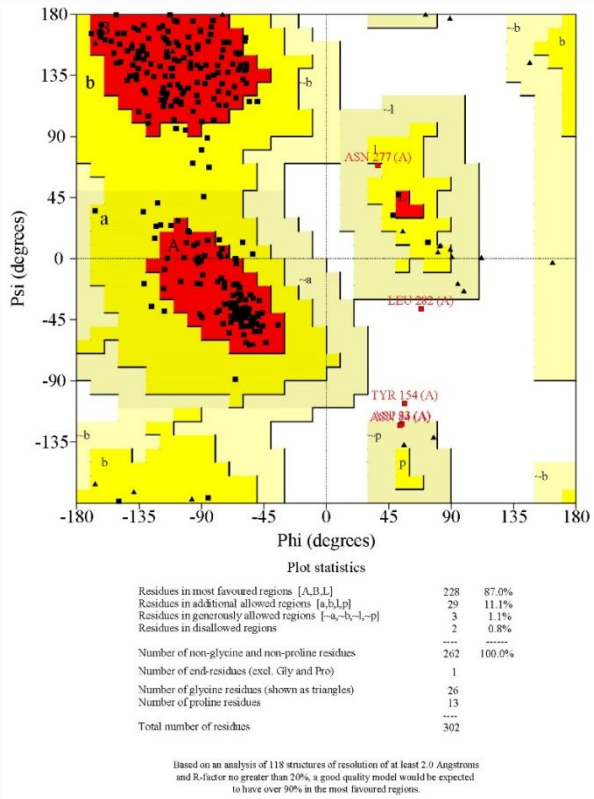

Figure1. Ramachandran Plot 2az5 obtained from PROCHECK server

The preparation of a protein involves importing of the SARS coronavirus main proteinase Protein structure. Binding pocket has been verified using PDBsum server which is a Pictorial database of 3D structures in the Protein Data Bank for interactions of standard inhibitor with protein. The water molecules, unnecessary chains and ligands have been deleted and the protein were retained using Biovia Discovery Studio visualizer V21.1.0.20298. Charges were stabilized,

missing residues were filled in and side chains were generated using AutoDockTools v1.5.6 spet_17_14.

The CHIMERA v1.5.3 software was used to minimize the structure of protein, using the Gasteiger charges with 1000 steepest descent steps of minimization.

Grid Generation

AutoDockTools was used for receptor grid identification. The prepared SARS coronavirus main proteinase was displayed in the Workspace. The volume of grid was calculated using dimensions of pocket identified from CASTp server (Computed Atlas of Surface Topography of proteins). The enclosing box was made small so that it will be consistent with the shape and character of the protein's active site and with the ligands that were expected to be docked.[26]

Ligands Preparation

Ligand molecules were designed in MarvinSketch v21.13 and saved in 3D MOL2 format. All the three compounds were processed, and optimized by UCSF Chimera v1.15 using AM1-BCC semi-empirical force field other parameters defaults like steepest descent steps : 1000; Conjugate gradient steps 100, etc.

Molecular Docking of Target Protein with Ligands

After obtaining the ligands and enzymes, their structures were converted to pdbqt format, using the AutoDock Tools 1.5.6 program, in which all the rotatable bonds of ligands were allowed to rotate freely, and the receptor were considered rigid. For docking studies, we used the AutoDock Vina 1.1.1, with 1 ˚A of spacing between the grid points. The grid box was centred on the active site of the enzyme with high resolution, allowing the program to search for additional places of probable interactions between the ligands and the receptor. Other configurations were considered default. The XYZ coordinates 70.627 X 36.344 X 20.769, and size of the grid box is 24 X 20 X 28 A^0. The redockings were performed with the same configurations of the previous performed dockings.

Visualization

Results obtained after Autodock Vina processing were subjected to make a complex using Biovia Discovery Studio visualizer. Interactions and binding energies of test compounds were compared with standard inhibitor.

Result:

All three compounds were prepared to dock with the Crystal Structure of SARS coronavirus main proteinase (PDB id 2ALV). The selected chemical structure of the the important ligands were shown in Figure 2.

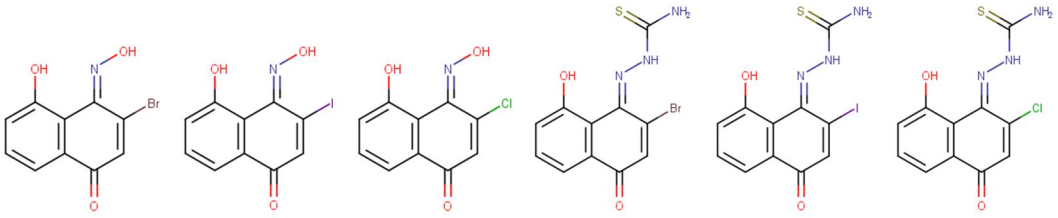

Figure 2. Structure of the Ligands

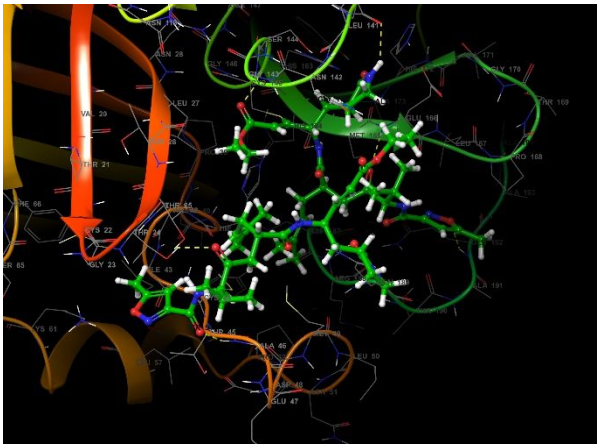

CY6

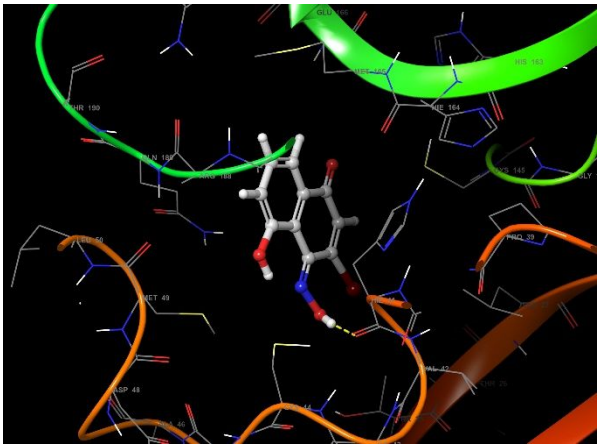

RM1

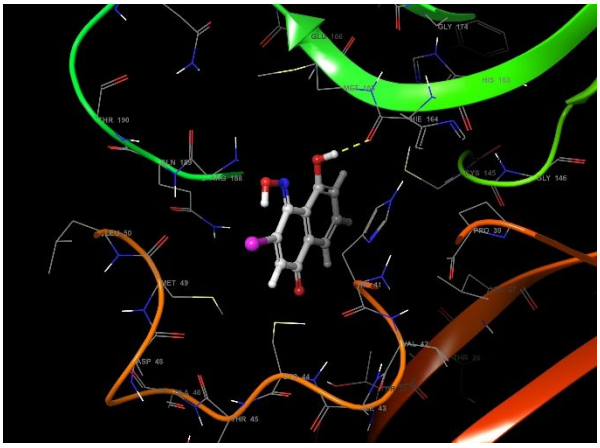

RM2

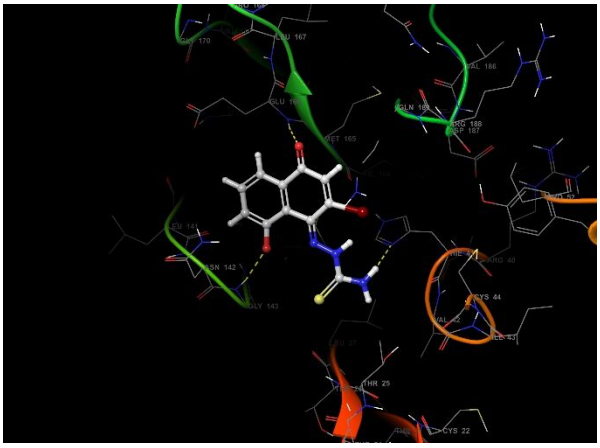

RM3

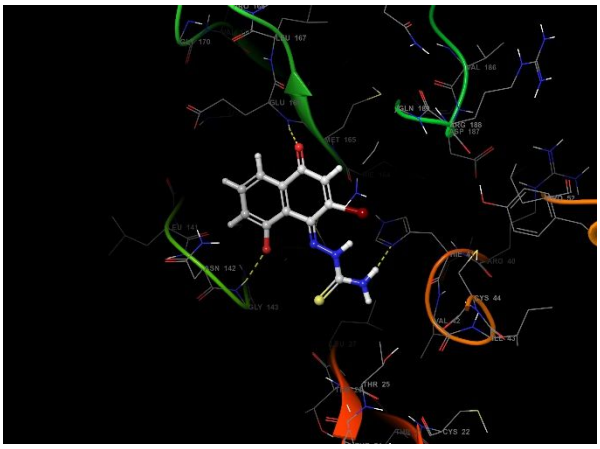

RM4

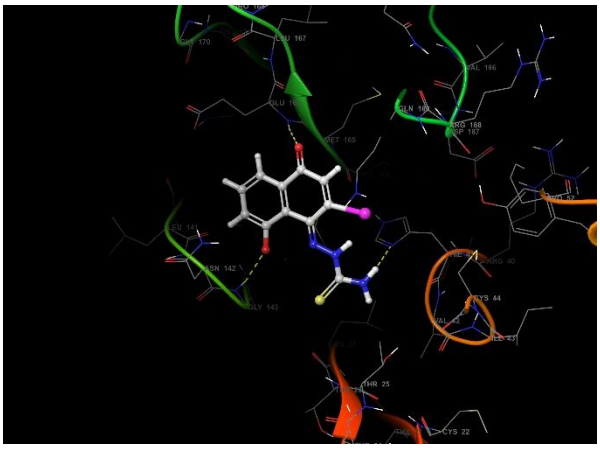

RM5

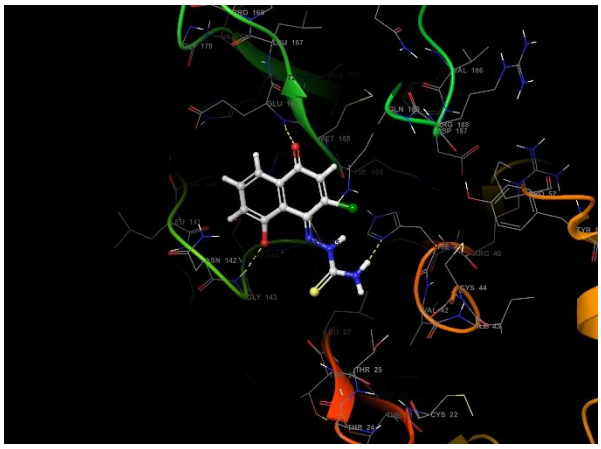

RM6

Figure 3. Docked conformation of ligands with 2ALV obtained from Maestro V12.8

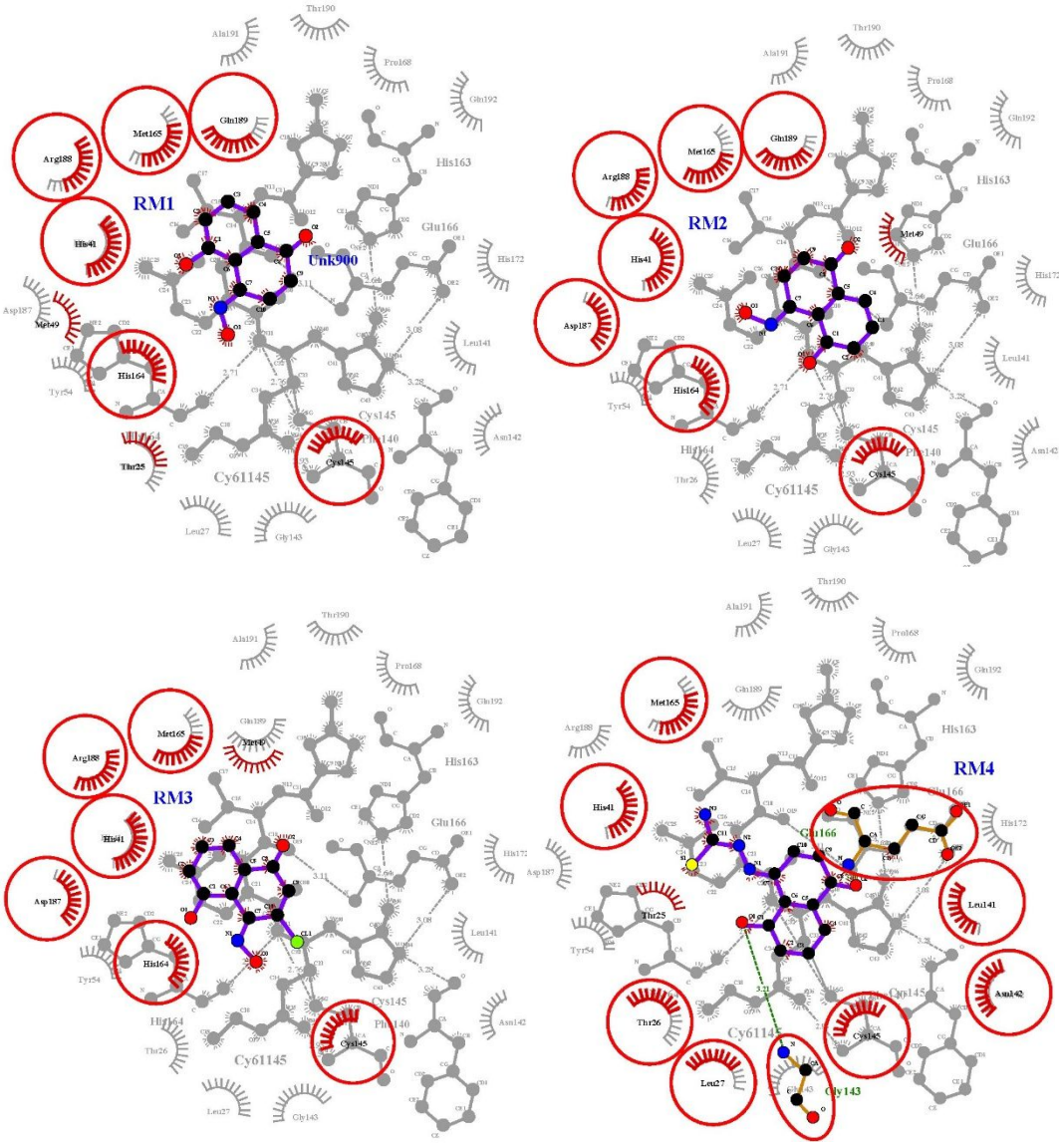

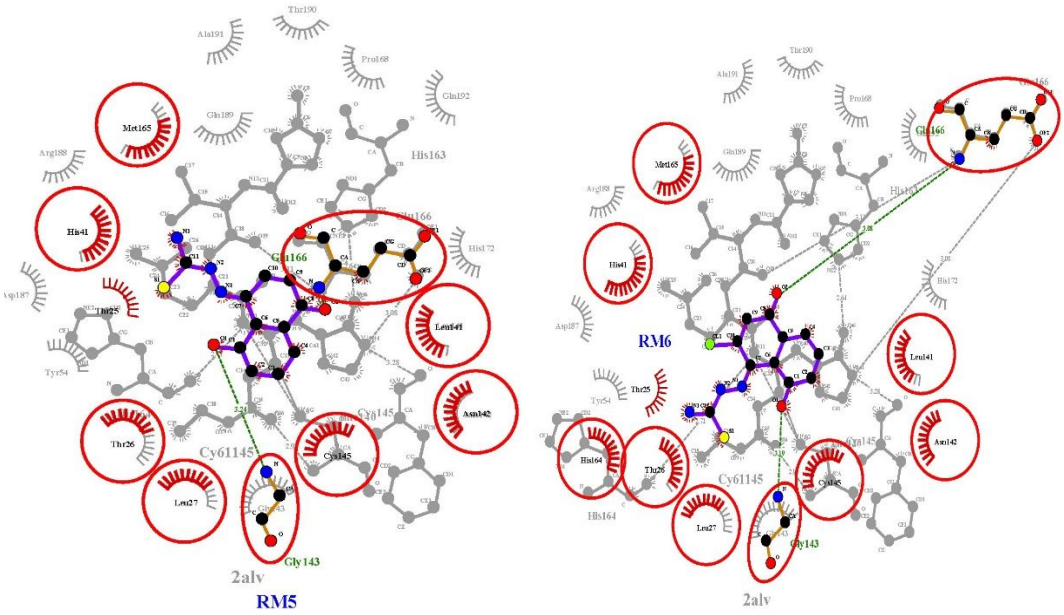

Figure 4. Overlapped 2D interactions images of designed compound compareds RM1 to RM6 with standard inhibitor CY6 at binding pocket of SARS coronavirus main proteinase.

Table 2. Docking Score and intermolecular interactions of ligands against SARS coronavirus main proteinase (PDB id 2ALV) using LigPlot v1.4.5, PLIP server, Maestro V12.8 and Biovia Discovery studio visualizer.

Name of compound	Binding energy	Type of interaction	Residue id	Distance (in A^0)
CY6 (standard)	-7.1	Hydrophobic	THR25A	3.77
			HIS41A	3.45
			PHE140A	3.55
			GLN189A	3.7
		Hydrogen bond	ASN142A	2.34
			GLY143A	3.08
			HIS163A	3.56
			GLU166A	3.44
			GLN189A	3.31
			GLN192A	3.14
RM1	-6.3	Hydrophobic Interactions	MET165A	3.75
			GLN189A	3.75
		Hydrogen bond	HIS41A	1.77
		π-Cation Interactions	HIS41A	3.80

RM2	-6.3	Hydrophobic Interactions	HIS41A	3.85
		Hydrogen bond	HIS164A ASP187A	2.81 3.62
		π-Stacking	HIS41A HIS41A	4.36 4.23
RM3	-6.3	Hydrophobic Interactions	HIS41A	3.80
		Hydrogen bond	HIS164A HIS164A	1.91 3.33
		π-Stacking	HIS41A	4.04
RM4	-6.2	Hydrophobic Interactions	GLU166A	3.67
		Hydrogen bond	HIS41A HIS41A GLY143A GLU166A	2.85 2.08 2.23 2.00
RM5	-6.2	Hydrophobic Interactions	GLU166A	3.68
		Hydrogen bond	HIS41A HIS41A GLY143A GLU166A	2.94 2.15 2.25 2.00
RM6	-6.1	Hydrophobic Interactions	GLU166A	3.74
		Hydrogen bond	HIS41A HIS41A GLY143A GLU166A	2.81 2.09 2.21 2.07

All the Six compounds were found to be binding with the SARS coronavirus main proteinase (PDB id 2ALV) and were used for further docking studies. The binding energy, type of interaction and their distances, interacted residues of protein with docked compounds are exhibited in Table. Compound id RM1, RM3 & RM6 exhibited good binding energy (-6.3) and formed H-bond with target as compared to standard inhibitor CY6 (-7.1) forming six hydrogen bond with five residues present in binding pocket of SARS coronavirus main proteinase (PDB id 2AZ5). The other three compounds RM2, RM4 and RM5 also having good binding affinity with protein -6.2, -6.2 and -6.1 respectively. From the above results it has been confirmed that all compounds have good affinity for SARS coronavirus main proteinase.

Molecular docking studies:

Molecular docking studies were performed to provide a theoretical perspective for possible molecular interactions of AB-series compounds and reference/ standard (CY6) molecules with the target proteins. The theoretical binding affinities were determined by energy minimization from docking calculation results. Molecular docking calculations were performed on Autodocktools version 4.2. energy minimization done using chimera, and molecular visualization of docking results were carried out by using the maestro.

Preparation of AB-series (ZG 1-7) and model inhibitor molecules for molecular docking was performed with MarvinSketch software. Before the docking process, the drawing and editing of the novel AB-series compounds in SD File format was done with the MarvinSketch suit program. These molecular structures have been protonated, added charges, and conformation minimization was performed with the root mean square gradient (RMS 0.001 kcal/mol/A2) by using the MMFF94 Forcefield parameters, which can be accessed in Energy Minimization protocols of these software.

Docking studies of AB-series compounds were carried out for important target structure named SARS-COV main protease from corona virus. The X-ray crystal structures as three-dimensional coordinates of these target proteins was obtained from the Research Collaboratory for Structural Bioinformatics (RCSB) Protein Data Bank. For use in docking
calculations, structures with PDB ID 2ALV was chosen as crystal structure model corresponding to target protein. Structural defects in target protein were eliminated automatically with the DeepView - Swiss-Pdb Viewer V 4.1 software provided by the SIB Swiss Institute of Bioinformatics. Then interactions of standard inhibitor supplied by depositor with protein were checked using PDBsum (Pictorial database of 3D structures in the Protein Data Bank) online server of European Bioinformatics Institute, UK from where position of ligand was noted. Other unnecessary entries present in pdb file were removed manually using textpad 8 software.

AutodockTools version 1.5.6 was used to optimize 3D module of protein. Then energy minimization of the system was performed with UCSF Chimera 1.12 using AMBER FF14SB by considering 1000 steepest descent steps & 100 conjugate gradient steps. Possible ligand binding site in the minimized protein were determined by Computed Atlas of Surface Topography of proteins (CASTp) server.

Molecular docking studies of selected compounds into protein targets were carried out using AutoDock Vina. Docking studies were conducted on SARS-CoV-2 main protease. For docking studies, proteins were pre-processed by removal of all water and addition of kollman charges. Hydrogen bond (H-bond) optimization was done and Gasteiger charges were added to it using AutoDock MGL tools 1.5.6. A receptor grid-box was generated by AutoGrid4 with grid box dimensions of 60 Å × 80 Å × 60 Å with spacing of 1 Å centering around hotspot residues Lys31, Glu35, Asp38, and Lys353 for ACE2 protein. Grid box for S-RBD was also set with spacing of 0.442 Å and dimensions of 62 Å × 82 Å × 82 Å centering around residues Leu455, Phe486, Asn487, Gln493, and Ser494. Lamarckian Genetic Algorithm (GA) in combination of grid based energy evaluation method was used for docking. The program was run for a total number of 50

Genetic algorithm runs. Other parameters were set as default and the final result obtained was analyzed manually by PyMol and LigPlot.

Docking of AB-series compounds and model inhibitors to the active site of these targets proteins was performed via AutodockTools 4.2 using the default docking calculation parameters. The average score of the top 10 final docking poses defined by the binding minimum energy (kcal/mol) for each compound was used as the final molecular docking score results. London dG scoring function was used for docking calculations. The London dG scoring function estimates the free energy of binding the ligand at a particular pose in a target structure. This scoring function is explained in detail in the user manual of the MOE software. After the initial scoring function for the obtained docking poses, the GBVI/WSA ΔG scoring function was used as the final docking scoring methodology. The GBVI/WSA dG is a force field-based scoring function, which estimates the free energy of binding of the ligand from a given pose [42]. This scoring function is explained in detail in the user manual of the MOE software.

Conclusion:

Interaction between Proteinase (PDB id: 2ALV) of corona virus and RM1 to RM6 studied by molecular docking. Negative value of ΔG indicates all compounds forms stable complexes with proteinase. RM1, RM2, RM3 shows better binding energy. It shows that changing halogen group does not showing any effects on complexation with proteinase. Oxime derivatives forms better complexes with proteinase than semicarbazide derivatives. Hydrogen bonding, electrostatic interactions,hydrophoboic and van der Waals interactions are studied.

Acknowledgement:

The authors thankful to SPPU,Fergusson College (Autonomous), B Gholap College and BJS ASC College for giving facilities for research work.

References:

[1]News Letter World Health organisation dated 6.10.2021

[2] S.H. Kim, K.S. Lee, J.K. Son, G.H. Je, J.S. Lee, C.H. Lee, C.J. Cheong, Cytotoxic compounds from the roots of Juglans mandshurica, J. Nat. Prod. 5 (1998) 643–645.

[3] A.M. Clark, T.M. Jurgens, C.D. Hufford, Antimicrobial activity of juglone, Phytother Res. 4 (1990) 11–14.

[4] R. Jin, A DFT study on the radical scavenging activity of juglone and its derivatives, J. Mol. Struc. -Theochem 939 (2010) 9–13.

[5] X.H. Peng, Y. Nie, J.J. Wu, Q. Huang, Y.Q. Cheng, Juglone prevents metabolic endotoxemia-induced hepatitis and neuroinflammation via suppressing TLR4/NF-kB signaling pathway in high-fat diet rat, Biochem. Bioph. Res. Co. 462 (2015) 245–250.

[6] X. Jin, Y.W. Zhang, Z.H. Zhang, D.B. Che, H.X. Lv, Juglone loaded poloxamer 188/phospholipid mixed micelles evaluated in vitro and in vivo in breast cancer, Int. J. Pharm. 515 (2016) 359–366.

[7]A.-M. Boudet, “Evolution and current status of research in phenolic compounds,” Phytochemistry, vol. 68, no. 22-24, pp. 2722–2735, 2007. [3] G. C. Fraga, Plant Phenolics And Human Health: Biochemistry, Nutrition And Pharmacology, John Whiley & Sons, NJ, USA, 2010.

[8] H. M. Mohamed, A. H. F. A. El-Wahab, A. M. El-Agrody et al., "Synthesis and characterization of new diiodocoumarin derivatives with promising antimicrobial activities," Beilstein Journal of Organic Chemistry, vol. 7, pp. 1688–1696, 2011.
[9] Study of fluorescent Eu(III) and Tb(III) Complexes with derivative of Lawsonemonoximes, **Sanjay Gaikwad**, *International Journal of Current Chemical Sciences (IJCCS)*, 5(9), 01-04, (2015),ISSN 2320 8146
[10] Bridging Precursors of Yttrium with Lawsonemonoximates, **Sanjay Gaikwad**, *Res. J. Chem. Environment*, 16 (4) (2012)
[11] Synthesis and Characterisation of Be(II) and Mg(II) complexes of 3-halolawsonemonoximes., **S. D. Gaikwad**, D. G. Kanse, V. D. Kelkar and B. A. Kulkarni. *Synth. React. Inorg. Met. Org. Chem*., 26 (9), 77-87 (1996)
[12] Synthesis and characterization of 2-TSCND and its –chloro derivative with Ni(II) **Sanjay Gaikwad***, Charushila Gaikwad, Sandip Khansole and Rajendra Kankariya, *Bulletien of Pure and Applied Science* 29C(No.1) 1 - 8 Jan – June (2010)
[13]Nickel Complexes of Thiosemicarbazone Derivatives of Lawsone, **Sanjay Gaikwad**, *Res.Rew. J. Chem*., Vol.2 (No. 3) pp 10-15 (2013)
[14] S. Salunke-Gawali, O. Pawar, M. Nikalje, R. Patil, T. Weyhermüller, V.G. Puranik, V.B. Konkimalla, Synthesis, characterization and molecular structures of homologated analogs of 2-bromo-3-(n-alkylamino)-1,4-napthoquinone, J. Mol. Struct. 1056–1057 (2014) 97–103.
[15] D. Chadar, M. Camilles, R. Patil, A. Khan, T. Weyhermüller, S. Salunke-Gawali, Synthesis and characterization of n-alkylamino derivatives of vitamin K3: Molecular structure of 2-propylamino-3-methyl-1,4-naphthoquinone and antibacterial activities, J. Mol. Struct. 1086 (2015) 179–189.
[16] D. Chadar, P. Banerjee, S. Kr. Saha, S. Bhand, R. Patil, S. Salunke-Gawali, n-alkylamino analogs of Vitamin K3: Electrochemical, DFT and anticancer activity of their oxidized and one electron reduced form, J. Mol. Struct. 1179 (2019) 443–452.
[17] R. Patil, S. Bhand, B. Konkimalla, P. Banerjee, B. Ugale, D. Chadar, S. Saha, P.P. Praharaj, C.M. Nagaraja, D. Chakrovarty, S. Salunke-Gawali, Molecular association of 2-(n-alkylamino)-1,4-naphthoquinone derivatives
[18] Zhao, Pan; Gao, Guihua; Zhang, Lianjun; Cai, Qian; Lu, Nan; Cheng, Li; Li, Shuaikang; Hou, Xiaohong (2017). *Drug-protein binding mechanism of juglone for early pharmacokinetic profiling: Insights from ultrafiltration, multi-spectroscopic and molecular docking methods. Journal of Pharmaceutical and Biomedical Analysis,* vol.4,pp 1541-1548,2017
[19] A.W. Schüttelkopf, D.M.F. van Aalten, PRODRG: a tool for high-throughput crystallography of protein-ligand complexes, Acta Crystallogr. Sect. D 60 (2004) 1355–1363.

Paper 72

Deposition and Characterization of CdSe Thin Film for Photovoltaic Applications

Sadekar H. K.

Department of Physics, Arts, Commerce and Science College, Sonai (MS)-India

Abstract

Cadmium selenide (CdSe) thin films were deposited by chemical bath deposition technique on glass substrates. Films were deposited at 80ºC bath temperatures. We determined structure of as-deposited thin films by X-Ray spectroscopy. Optical properties of as deposited films were studied by absorption spectra. The optical absorption spectra showed a band gap is of 1.74 eV. The scanning electron microscope (SEM) study indicates that grain size increases with increase of bath temperature. The study of physical, optical and electrical properties reveal that the CdSe thin film can be suitably employed in Photovoltaic applications.

1. Introduction

Thin films of II–VI group compound semiconductors, due to their direct and large band gap, have promising applications in optoelectronics and photo-voltaic devices [1,2]. Cadmium Selenide (CdSe) is a II–VI group compound semiconductor, which has promising optoelectronic properties, make it suitable for various applications in the field of low-cost optoelectronic devices such as photoconductors [3], LEDs [4] and photovoltaic solar cells [5,6]. The CdSe thin films have been deposited by various techniques, such as electron beam evaporation [7], r. f. magnetron sputtering [8], molecular beam epitaxy [9], spray pyrolysis [10], SIILAR [11], chemical bath deposition [12,13]. Chemical bath deposition is a method of growing thin films of certain materials on a substrate immersed in an aqueous bath containing appropriate reagents at temperatures ranging from room temperature to 100°C. In this study, we report the preparation of CdSe thin films onto microscope glass slides by CBD method. The structural, morphological and optical properties of the as-prepared films are investigated.

2. Experimental

2.1Thin Film Preparation

The CdSe thin films were deposited using mixture of aqueous solutions of cadmium sulphate, selenium powder, sodium sulphite, trisodium citrate, triethanolamine (TEA), hydrazine hydrate, and sodium hydroxide (NaOH), where TEA was used as the complexing agent and sodium hydroxide for adjusting the pH. The substrates used for the deposition of

CdSe thin films were commercial microscope glass slides (Blue Star) with the size of 75 x 25 x 1.35 mm. Before deposition, the substrates were degreased in HNO_3 solution for 24 h, cleaned by commercial detergent and finally rinsed with de-ionized water and dried in desiccator. This process was carried to ensure clean surface, essential for formation of nucleation centers required for thin film deposition. All chemicals used in the present investigations were AR grade. Aqueous solutions of 0.5 M cadmium sulphate ($CdSO_4$), 0.5 M sodium selenosulphate (Na_2SeSO_3), 0.4 M trisodium citrate, triethanolamine (TEA), 80 % hydrazine hydrate and 5 M sodium hydroxide (NaOH) were used to prepare thin films. Sodium selenosulphate was prepared by refluxing 0.5 M selenium powder mixed with 1 M sodium sulphite in de-ionized water, which was heated to 80 °C for 8 h [14]. Cadmium sulphate solution (20 mL) was taken in a 50 mL glass beaker to which 30 drops of TEA, 5 mL NaOH and 5 drops of hydrazine hydrate solutions were added slowly under continuous stirring. Initially, the solution was milky and turbid due to the formation of $Cd(OH)_2$ suspension. Addition of excess NaOH led to the dissolution of turbidity and made the solution clear and transparent. Then 5 mL trisodium citrate and 20 mL freshly obtained sodium selenosulphate solutions were added slowly with constant stirring. pH of the final mixture was adjusted to ~ 13. Pre-cleaned glass substrates were inserted into the reaction mixture standing parallel with the walls of the beaker, which was kept in constant temperature bath for 4 h at 80° C. Thereafter, the substrate coated with CdSe was removed, rinsed with distilled water, and dried in desiccator. It was observed that the film was uniform, well adhered, and reddish in color [15]. Adhesion of the film was confirmed by centrifugal method. Thickness of the film was found to be ~ 300 nm by using weight difference method. It is noted that the growth is highly dependent on temperature and concentration of complexing agent.

2.2 Characterization techniques

As-deposited thin film of CdSe was characterized for structural, optical and electrical properties. Glancing incidence angle X-ray diffraction (GIXRD) pattern of the film was recorded on a Bruker AXS, Germany (D8 Advanced) diffractometer. The scanning range of diffractometer used is 20–80° (2θ), using Cu-$K_{\alpha 1}$ radiations with wavelength 1.5405 Å at 0.5° The surface morphology was studied by scanning electron microscopy (SEM, JOEL-JSM-5600). Transmittance and absorbance spectra were recorded in the range 300–1000 nm by means of Jasco V630 spectrophotometer. The resistivity of the films was determined by four probe method.

3. Results and discussions

3.1 Structural and Compositional Studies

Fig. 2 shows X-ray diffraction pattern of as-deposited CdSe thin film. The XRD peaks indicate that the film is polycrystalline in nature. The 2θ peaks 25.30°, 42.2° and 49.70° corresponds to reflection from (111), (220) and (311) planes, respectively. The (111) plane is the preferred orientation and it is the close-packing direction of the zinc-blend structure of cubic CdSe phase (JCPDS card No 91-0191). Crystallite size (D) of the film was calculated using Scherrer's formula [8] from the full width at half maxima (β) of the peakes expressed in radians,

$$D = \frac{K\lambda}{\beta Cos\ \theta} \qquad (1)$$

where 'K' is constant dependent on crystallite shape (0.89), 'λ' is wavelength of $CuK_{\alpha 1}$ radiation, and 'θ' is angle between the incident and scattered X-rays. The average crystallite size (derived from Fig. 2) is found to be < 100 nm.

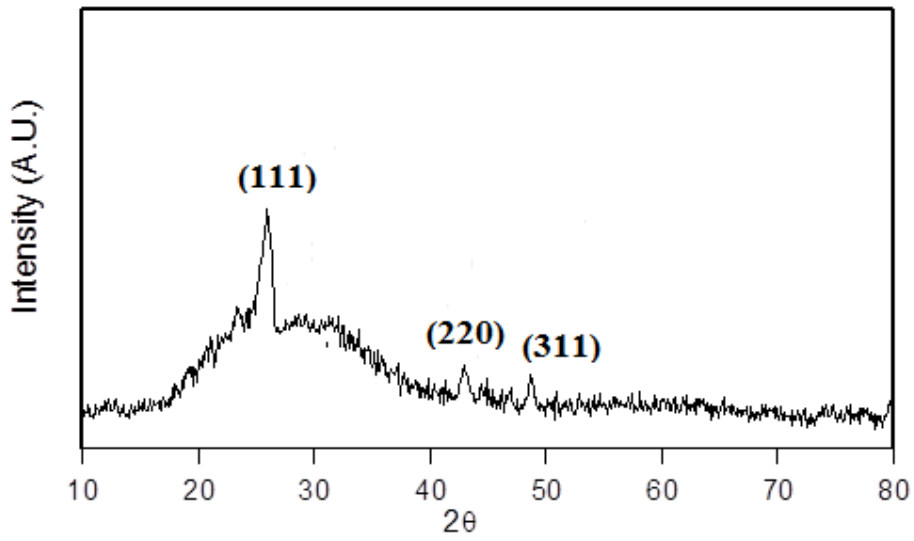

Figure. 1. GI XRD pattern spectrum obtained from the as-deposited CdSe thin film.

3.2 Surface morphological and topographical Studies

Fig. 2 shows a. SEM image of the as-deposited ZnSe film which confirms, uniform deposition. The fine grains were well defined, spherical with different sizes and were uniformly distributed over a smooth homogeneous background corresponding to the nanocrystalline phase of CdSe. Some of the grains are seen to be united/fused forming agglomerates and the grain size obtained from SEM is about ~ 100 ± 20 nm.

Figure. 2. SEM image of 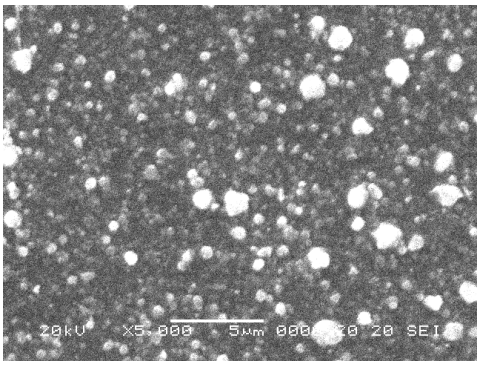 as-deposited CdSe thin film

3.3Optical Studies

Fig. 3a inset shows transmittance and absorbance spectra obtained from as-deposited CdSe thin film. The optical transmittance of over 65% is noted in the visible region. The relation between the absorption coefficient α and the incident photon energy (hν) [8] can be written as,

$$\alpha h\nu = A(h\nu - E_g)^n \qquad (2)$$

where 'A' is constant, n= ½ for direct allowed transition, 'E_g' is optical band gap of the material. Fig. 3b shows the plot of $(\alpha h\nu)^2$ against (hν) for CdSe thin film derived from the absorbance spectra. Extrapolating the straight-line portion of the plot of $(\alpha h\nu)^2$ vs (hν) for zero absorption coefficient value gives the band gap, which is found to be 1.74 eV at room temperature.

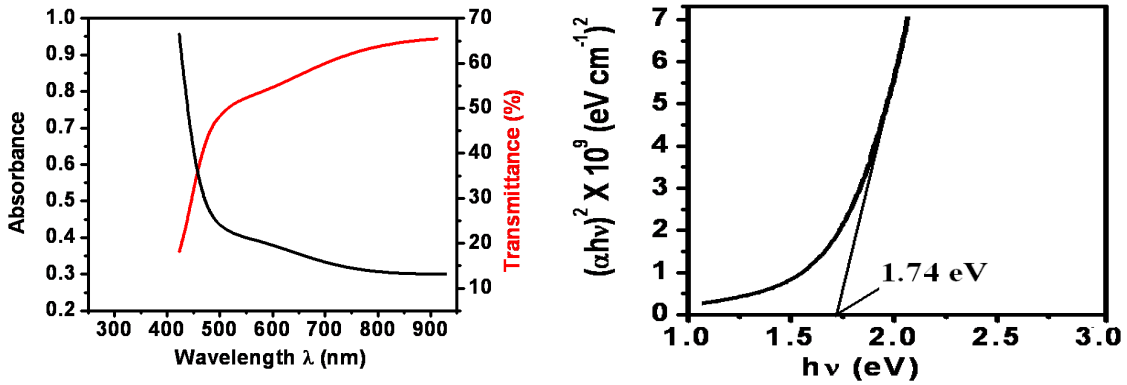

Figure. 3. (a) Plot of absorbance and transmittance versus wavelength, (b) Plot of $(\alpha h\nu)^2$ versus (hν) obtained from as-deposited CdSe thin film.

4. Conclusion

CdSe thin film were grown using ammonia free precursor solutions with appropriate selection of the growth parameters by inexpensive CBD. The as-deposited film present

excellent adherence, uniform deposition, smooth morphological and nanocrystalline properties, confirmed by SEM and XRD analysis. It is found that the as-deposited CdSe films are highly oriented with cubic zinc blende structure, and the preferred crystal orientation is (111) plane. The XRD FWHM also suggests that the crystal quality of the as-deposited CdSe films is reasonably good. The EDAX study shows almost stoichiometric deposition. Energy band gap of the asdeposited CdSe film is 1.74 eV and it is quite close to the reported value of 1.88 eV, which shows a blue emission. The study of physical, optical and electrical properties reveal that the CdSe thin film can be suitably employed in Photovoltaic applications.

Acknowledgements

We are thankful to Dr. Shankar Laware, Principal, Arts, Commerce and Science College, Sonai and Dr. Ramphal Sharma, Professor, Dr. B.A.M.U. Aurangabad for support of laboratory facility. Special thanks to Dr. D. M. Phase, Dr. V. R. Reddy, Dr. V. Ganesan, UGC-DAE, and Consortium for scientific research, Indore for characterization support.

References

1. A. M Souad, Al-Bat'hi, Yose Fachmi Buys, Materials Today: Proceedings **3** (2016) 2832–2840.
2. G. GordilloT, E. Romero, Thin Solid Films 484 (2005) 352– 357.
3. Sung-Gi Hur et al., Journal of Vacuum Science & Technology B 26 (2008) 1334-1337.
4. N. Gupta et al., Organic Electronics **34** (2016) 276-283.
5. L. Tian et al., Current Applied Physics **14** (2014) 881-885.
6. R.P. Dutta and N. Neog, Materials Today: Proceedings **42** (2021) 893–896
7. S. Mathuri et al., Thin Solid Films, https://doi.org/10.1016/j.tsf.2018.05.041
8. H.N. Rosly et al., Superlattices and Microstructures, https://doi.org/10.1016/ j.spmi.2020.106716.
9. Q.Yang, J. Zhao et.al, Applied Surface Science, **257(21)** (2011) 9038-9043.
10. A. A. Yadav, M. A. Barote,E.U. Masumdar, Solar Energy, **84(5)** (2010) 763-770.
11. K.B. Chaudhari, N.M. Gosavi, N.G. Deshpande, S.R. Gosavi, Journal of Science: Advanced Materials and Devices **1** (2016) 476-481.
12. A.A. Abdulwahab et al., Optik, **236** (2021) 166659.
13. F. Garibay-Martínez et al., Optik, Optik **242** (2021) 167284.
14. H. K. Sadekar, A. V. Ghule, R. Sharma, J. Alloys Compd., **509** (2011) 5525-5531.
15. A.G. Habte, F.G. Hone and F.B. Dejene, Inorganic Chemistry Communications, https://doi.org/10.1016/j.inoche.2019.03.017

Paper 73

Insillico Prediction of Novel Halosubstituted Homoisoflavonoid Derivatives as an Anti-Inflammatory Agents.

Dinesh Gaikwad and Sanjay Gaikwad
Bharatiya Jain Sanghatana's Arts, Science and Commerce College, Wagholi, Pune

Abstract:

Flavonoids are class of organic compounds derived from families of plants like Hyacinthaceae, Fabaceae, Aspargaceae. These compounds are phenolic secondary metabolites having skeleton C_6-C_3-C_6 and have 15 carbon atoms containing aromatic rings. Homoisoflavonoids are small group of natural flavonoids containing 3-benzyl-4-chromanones reported to occur mainly in the genera in in Hyacinthaceae. In the present study, we have synthesized hydroxy and nitro derivatives of chloro substituted homo isoflavonoids. The structures of of synthesized compounds were confirmed by H1 NMR and IR spectral techniques.

Naturally occurring homoisoflavonoids are extensively used in medication and their biological activities are reported such as antiinflammatory obtaining antioxidant, antifungal and anticancer drugs. In our work we have synthesized novel synthetic hydroxy and nitro derivative of chloro substituted homoisoflavonoids and their insillico anti-inflammatory activities are studied and compared using molecular docking.

Introduction

In ancient time humans use medicinal plants and there extract in the form of of tinctures and lotions for medication purpose. Plants produce primary and secondary metabolites. Secondary metabolites include alkaloids, glycosides, amines, steroids and flavonoids. Recently the secondary metabolites homoisoflavonoids is small subclass from class of flavonoids widely used in in drug medication. Homoisoflavonoids are generally known to contain 3-benzyl-4-chromanones backbone. These compounds are widely used studied as a anti-inflammatory drugs and for different biological activities. The Anti-inflammatory activities of novel hydroxy and nitro derivatives of chloroisoflavonoids can be predicted insillico study by molecular docking. Activity spectra prediction is done using pass online module of "Way to drug" server.

For docking study protein was isolated from Research collaborator for Structural Bioinformatics (RCSB) online database. Then protein and ligands optimized using various softwares. Grid parameters obtained from Cast- P –server.

Actual docking one using Auto.Doc tools 4.2. Analysis of protein ligand complex obtained by docking using "Discovery studio" lig plot and Maestro. On the basis of comparative anti-inflammatory study, H- bond and other electrostatic forces forming compounds shows better affinity towards receptor.

Experimental

Synthesis of homoisoflavonoids

The compound 3-(3,5-dichlorophenoxy) propanoic acid(A) is synthesized from 3,5-Dichlorophenol by the action of NaH and 3- Bromopropanoic acid in DMF. Further in step -2 compound (A) is treated with polyphosphoric acid to give 5,7-dichloro-2,3-tetrahydro-4H-chromen-4-one. In step-3 compound B is treated with -ortho, -meta and -para hydroxyl and

nitro benzaldehyde to get hydroxyl and nitro substituted chlorohomoisoflavonoids. The purity of compounds were checked using TLC. The characterization of compounds was carried out using IR, H^1 NMR and mass spectroscopy.

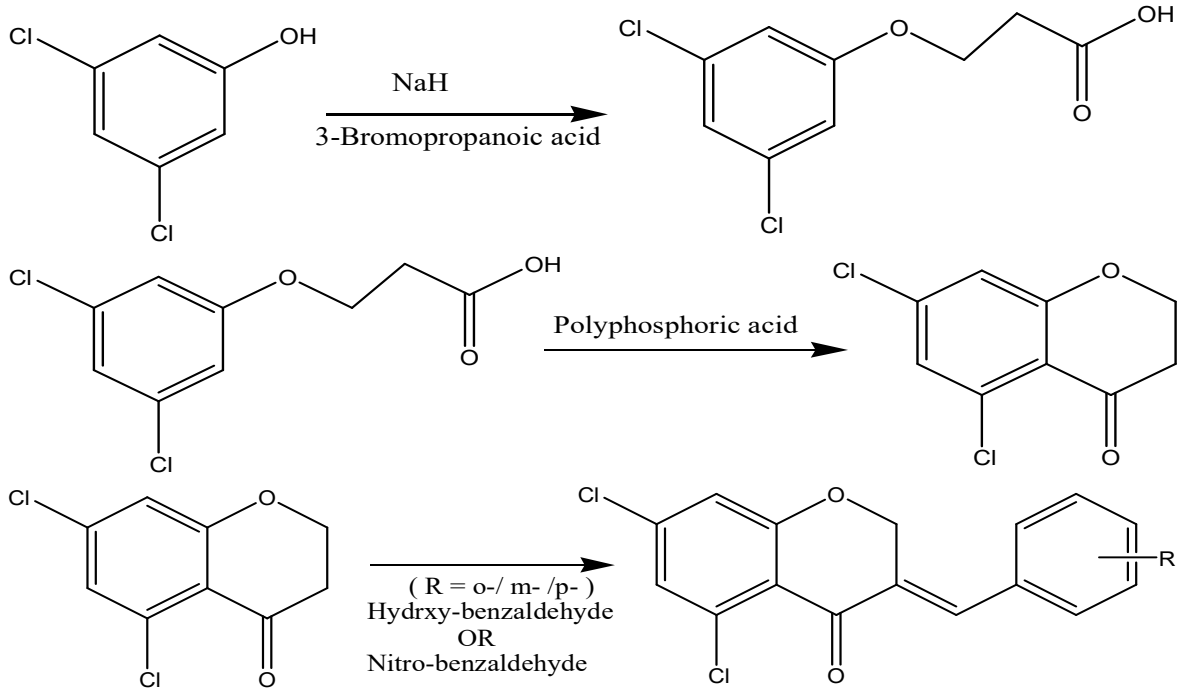

Methodology, Result and Discussion

Selection of particular Ligands from Homoisoflavonoids derivatives

The important derivatives from synthesized compounds were used in the present investigation for the computational prediction of potential drugs from it by the process of molecular docking against COX-2 isoenzyme as an anti-inflammatory agent.

Biological Activity Prediction

Due to the impossibility of performing a study of the biological activity of a large number of compounds in a short period, it was decided to conduct a preliminary assessment of the potential biological activity of compounds (DG1, DG2, DG3, DG4, DG5 & DG6) using PASS-online modelling. The PASS software product, which predicts more than 300 pharmacological effects and biochemical mechanisms on the basis of the structural formula of a substance, may be efficiently used to find new targets (mechanisms) for some ligands and, conversely, to reveal new ligands for some biological targets. The mean accuracy of prediction with PASS is about 86% in LOO cross-validation. The tool uses the descriptors to predict the activity of a substance.

Result

The prediction of the biological activity spectrum of homoisoflavonoid derivatives **DG1 to DG6** revealed that compounds are determined as promising selective cox-2 inhibitors. This indicates that all the compounds may show good anti-inflammatory activity as selective COX-2 inhibitor.

The 3D SDF structures of the processed six Homoisoflavonoid derivatives **RM1 to RM6** were given as an input for PASS server. The PASS server provides all the possible activities of the given Homoisoflavonoid derivatives as promising COX-2 inhibitors. PASS

can be effectively applied to predict biological potential of compounds and to analyze large chemical databases. PASS predicted search results show all the available information on the pharmacological and toxicological activity of all the three compounds analysed. Similar observation in accordance with the present study using PASS server was already reported by many researchers. Pa and Pi are the estimates of probability to be active and inactive respectively from the biological activity spectrum. Their values vary from zero to one. Each active compound possesses a number of biological activities. Its specificity of action is always relative and is defined by the peculiarities of object, dose, route, etc. Biological activity spectrum of compound can be predicted on the basis of structure-activity relationships found by the analysis of the known data from the training set. Based on the analysis of large training set consisting of tens of thousands of the known biologically active compounds, computer program PASS provides the means to evaluate any new compound in huge chemical-pharmacological space. On the basis of this study it can be reveals that all the three compounds may show good anti-inflammatory activity

Molecular Docking Studies

Target Protein Retrieval and Preparation

On the basis of literature survey we found that COX-2 isoenzyme is major target to study anti-inflammatory study. Therefore, fasta sequence of cyclooxygenase-2 (Prostaglandin-endoperoxide synthase 2) for Homo sapience was retrieved from National centre for biotechnology information server and done Basic Local Alignment Search for regions of similarity between biological sequences available on Protein Data Bank. Then Three-dimensional X-Ray crystallographic structure of COX-2 (PDB id: 5F1A) was obtained from PDB databank which was validated using various parameters like resolution, Mutation and Ramachandran plot. Details are as follows.

Table 1. Comparison between standard values and retrieved protein for validation of protein selected for docking study

Parameters	**Details**	**Standards**
Protein Id and method of experiment	5F1A X-RAY Diffraction	- X-RAY Diffraction
Mutation	No	No
Resolution	2.38 A^0	Near about 2.00 A^0
Ramchandran Plot (by PROCHECK server) Residues in favoured + Allowed regions	100%	>88 %

The preparation of a protein involves importing of the Prostaglandin-endoperoxide synthase 2 Protein structure. Binding pocket has been verified using PDBsum server which is a Pictorial database of 3D structures in the Protein Data Bank for interactions of standard inhibitor with protein. The water molecules, unnecessary chains and ligands have been deleted and the proteins were retained using Biovia Discovery Studio visualizer V21.1.0.20298. Charges were stabilized, missing residues were filled in and side chains were generated using AutoDockTools v1.5.6 spet_17_14.

The CHIMERA v1.5.3 software was used to minimize the structure of protein, using the Gasteiger charges with 1000 steepest descent steps of minimization.

Grid Generation

AutoDockTools was used for receptor grid identification. The prepared Prostaglandin-endoperoxide synthase 2 was displayed in the Workspace. The volume of grid was calculated using dimensions of pocket identified from CASTp server (Computed Atlas of Surface Topography of proteins). The enclosing box was made small so that it will be consistent with the shape and character of the protein's active site and with the ligands that were expected to be docked.

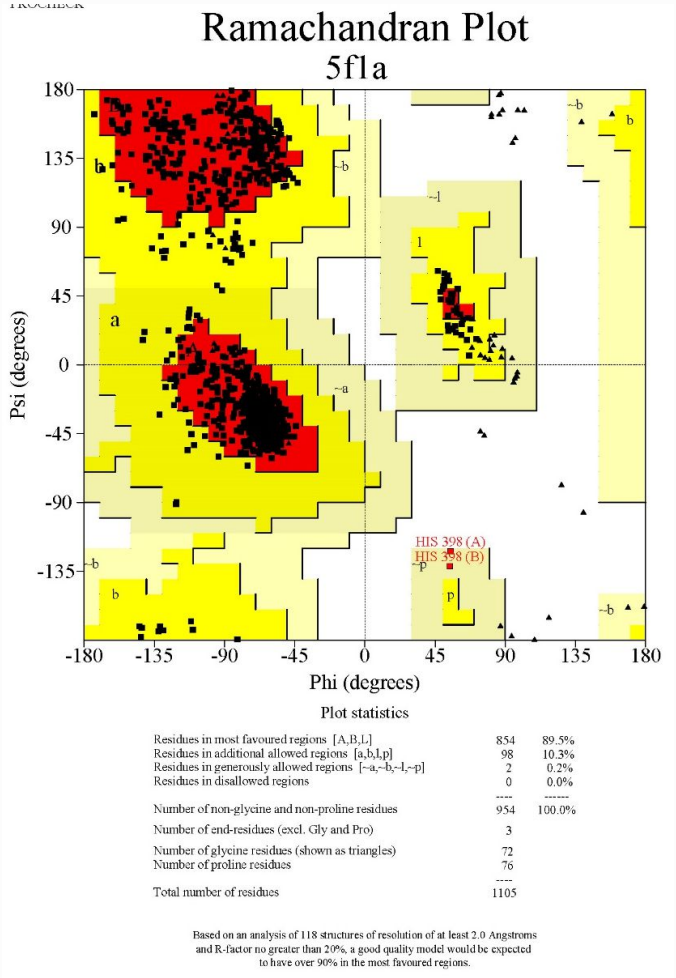

Figure 1. Ramachandran Plot 5F1A obtained from PROCHECK server

Ligands Preparation

Ligand molecules were designed in Marvin Sketch v21.13 and saved in 3D MOL2 format. All the three compounds were processed, and optimized by UCSF Chimera v1.15 using AM1-BCC semi-empirical force field other parameters defaults like steepest descent steps : 1000; Conjugate gradient steps 100, etc.

Molecular Docking of Target Protein with Ligands

After obtaining the ligands and enzymes, their structures were converted to pdbqt format, using the AutoDock Tools 1.5.6 program, in which all the rotatable bonds of ligands were allowed to rotate freely, and the receptor were considered rigid. For docking studies, we used the AutoDock Vina 1.1.1, with 1 ˚A of spacing between the grid points. The grid box was centred on the active site of the enzyme with high resolution, allowing the program to search for additional places of probable interactions between the ligands and the receptor. Other configurations were considered default. The XYZ coordinates 41.81 X 23.95 X 240.11, and

size of the grid box is 20 X 20 X 20 A^0. The redockings were performed with the same configurations of the previous performed dockings.

Visualization

Results obtained after Autodock Vina processing were subjected to make a complex using Biovia Discovery Studio visualizer. Interactions and binding energies of test compounds were compared with standard inhibitor.

Result

All three compounds were prepared to dock with the Crystal Structure of Prostaglandin-endoperoxide synthase 2 (PDB id 5F1A). The selected chemical structures of the three important ligands were shown in Fig.

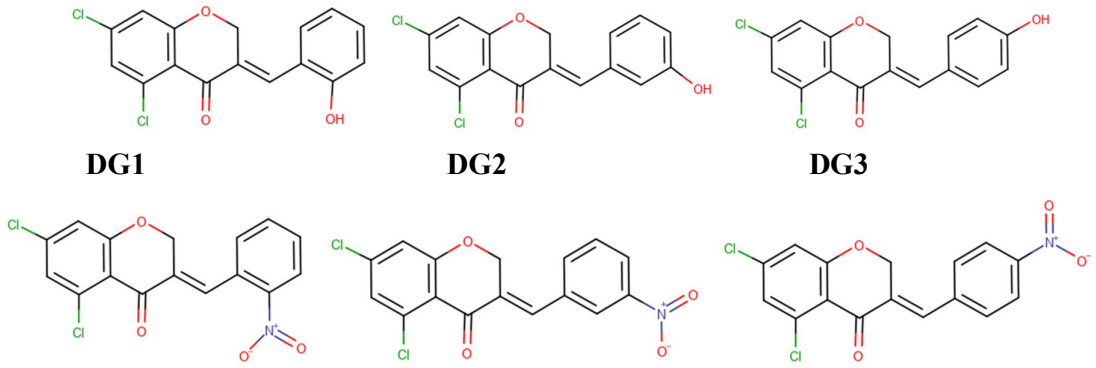

Figure 2.: 2D structure of ligands drawn in Marvin Sketch

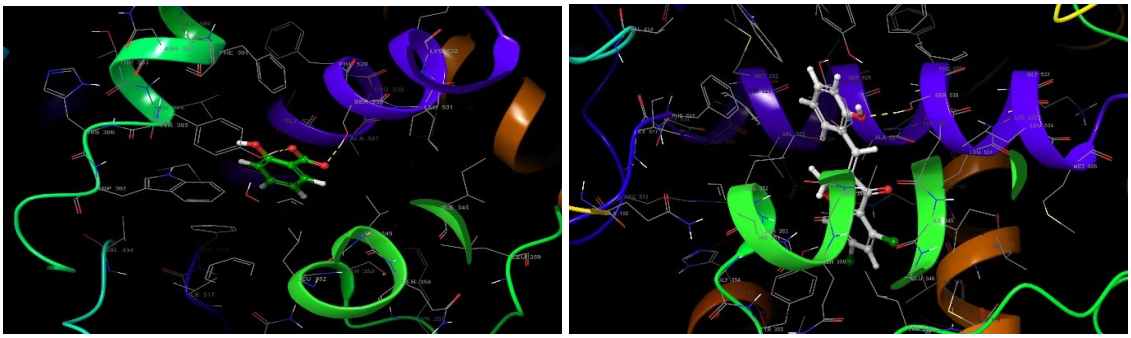

SAL **DG**1

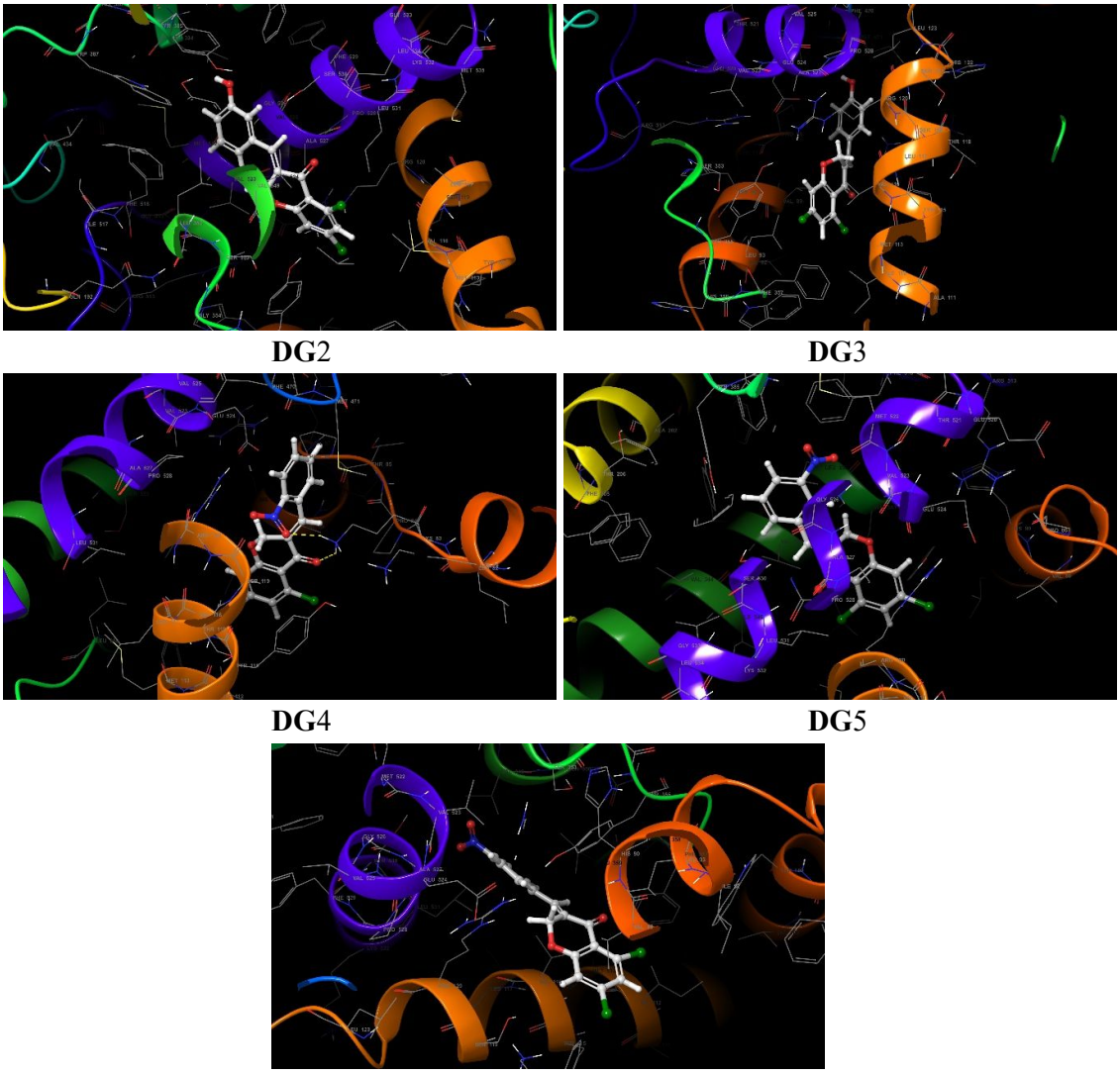

Figure 3. Docked conformation of ligands with 5F1A obtained from Maestro V12.8

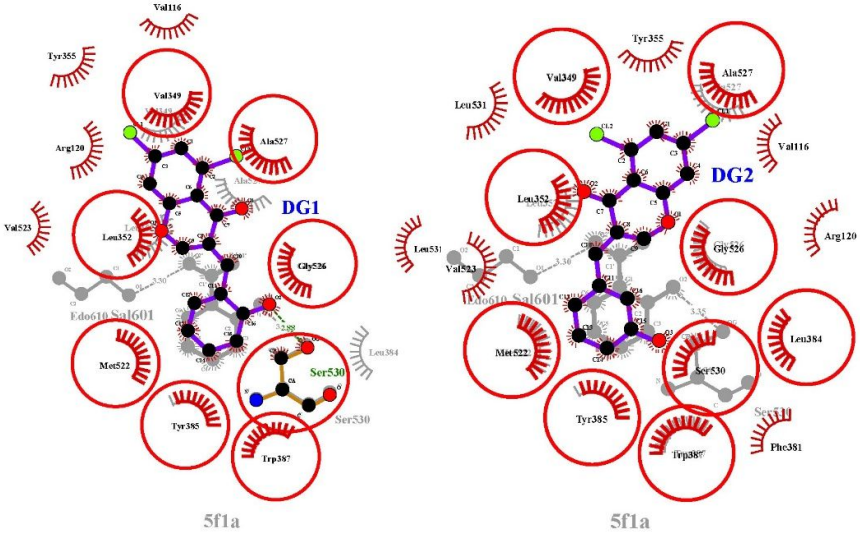

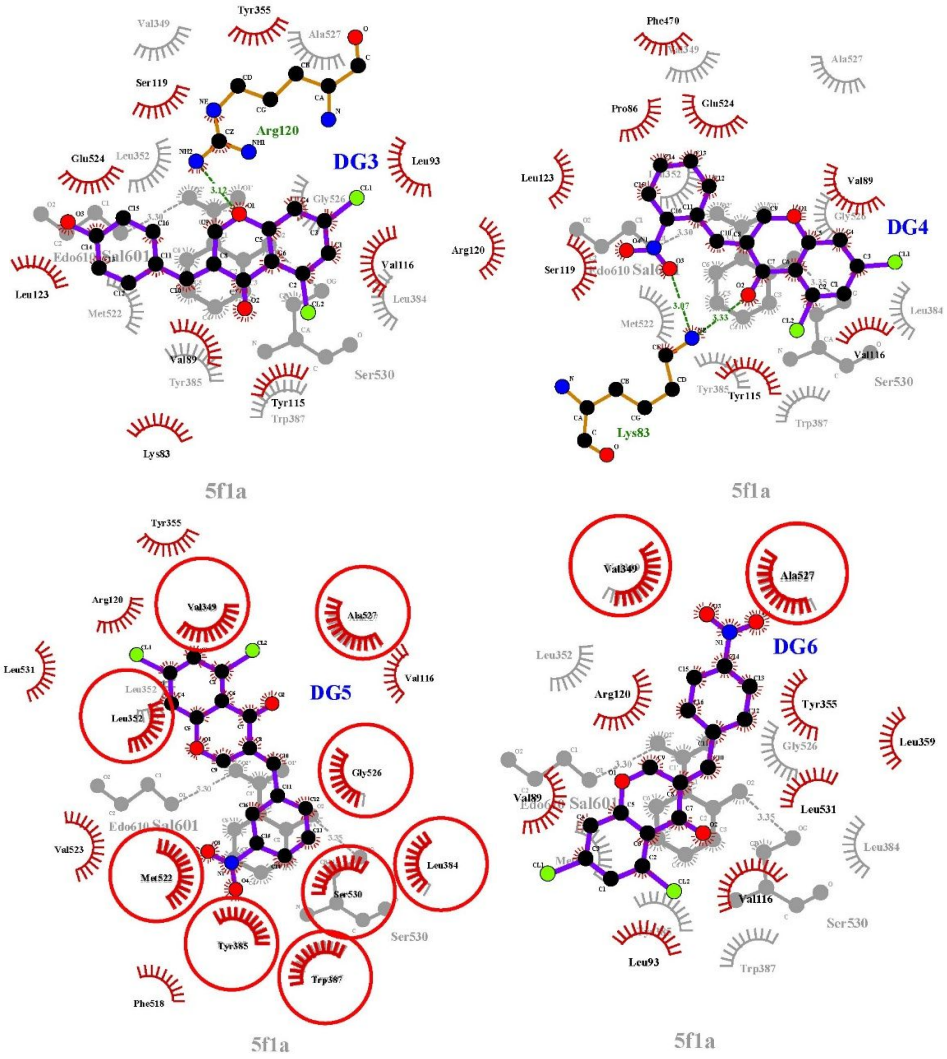

Figure 4. Overlapped 2D interactions images of designed compound compared DG1 to DG6 with standard inhibitor SAL at binding pocket of Prostaglandin-endoperoxide synthase 2

Table 2. Docking Score and intermolecular interactions of ligands against Human Cyclooxygenase-2 (PDB id 5F1A) using LigPlot v1.4.5, PLIP server, Maestro V12.8 and Biovia Discovery studio visualizer

Name of compound	Binding energy	Type of interaction	Residue id	Distance (in A^0)
SAL (standard)	-6.935	Hydrophobic	LEU 352A TRP 387A PHE 518A	3.54 3.63 4.00
		Hydrogen bond	TYR 385A SER 530A	1.94 1.78
DG1	-7.414	Hydrophobic Interactions	VAL 116A VAL 349A	3.27 3.43 3.61 3.80

			TRP 387A TRP 387A ALA 527A	3.25
		Hydrogen bond	TYR 355A TYR 385A TYR 385A SER 530A	3.48 3.30 3.14 1.94
DG 2	-7.505	Hydrophobic Interactions	VAL 116A LEU 352A TRP 387A ALA 527A	3.31 3.94 3.52 3.33
DG 3	-4.463	Hydrophobic Interactions	VAL 89A TYR 355A	3.68 3.83
		Hydrogen bond	ARG 120A ARG 120A PHE 470A	3.13 2.69 2.74
		π-Cation Interactions	ARG 120A ARG 120A PHE 470A	3.13 2.69 2.74
DG 4	-5.074	Hydrophobic Interactions	PRO 86A LEU 93A TYR 115A VAL 116A LEU 123A LEU 472A	3.58 3.96 3.74 3.61 3.69 3.98
		Hydrogen bond	LYS 83A	2.45
DG 5	-6.533	Hydrophobic Interactions	VAL 116A VAL 349A VAL 349A LEU 352A TYR 385A TRP 387A ALA 527A	3.26 3.90 3.39 3.94 3.86 3.49 3.27

		Hydrogen bond	TYR 355A	3.49
DG 6	-4.363	Hydrophobic Interactions	VAL 116A VAL 349A TYR 355A LEU 359A ALA 527A LEU 531A	3.10 3.52 3.25 3.69 3.24 3.35
		Hydrogen bond	ARG 120A ARG 120A	3.64 3.25

From All the Six compounds were found to be binding with the Human Cyclooxygenase-2 (PDB id 5F1A) and were used for further docking studies. The binding energy, type of interaction and their distances, interacted residues of protein with docked compounds are exhibited in Table 2 Compound id DG1 & DG2 exhibited good binding energy and intermolecular interactions with respect to standard inhibitor Salicylate. The other four compounds DG3, DG4, DG5 & DG6 also having moderate binding affinity with protein. From the above results it has been confirmed that compounds with meta-hydroxy and ortho-hydroxyl derivatives of homoisoflavonoids have good affinity for Prostaglandin-endoperoxide synthase 2. We can conclude from docking study that homoisoflavonoids with Electron donating groups has good binding affinity than electron withdrawing groups.

Acknowledgment

The authors are thankful to SPPU, Pune, department of Chemistry, BJS College, Wahgoli, Pune, B R Gholap College, Sangavi, Pune for allowing the facilities to do research work

References

1. Oshiro, C., Bradley, E.K., Eksterowicz, J., Evensen, E., Lamb, M.L., Lanctot, J.K., Putta, S., Stanton, R. and Grootenhuis, P.D., 2004. Performance of 3D-database molecular docking studies into homology models. *Journal of medicinal chemistry*, *47*(3), pp.764-767
2. Harborne, J.B.; Mabry,T.J.; *The flavonoids advances in Research*, **1982**, 1975-81.
3. Williams C.A.; Harborne J. B.; Glassman, S.F.; *Plant Syst. Evol.***1983**, 142; 157-169.
4. Cragg, G.M, Newmann,D, *J Pharmaceutical Biology,***2001**,39,8-17
5. Mahidansha M. Shaikh et.al. Hendrik G. Kruger, Peter Smith, Orde Q. Munro, Johannes Bodenstein, Karen du Toit, *Natural product Research*, 26:16 , **2012**,1473-1482.
6. L. Lin, Q.Y. Liu , Y. Ye, *Planta medica.*, **13,** 1053-66 (2014)
7. V. Siddaiah, C. V. Rao, S. Venkateswarlu, A. V. Krishnaraju, G. V. Subbaraju, *Bioorganic and medicinal chemistry*., **14(8),** 2545-51 (2006).

8. U. Snekhalatha, M. Anburajan, B. Venkatraman, M. Menaka, Z *Rheumatol*., **72(4),** 375-82 (2013).
9. M. M. Hossain, M. S. Kabir, A. Hasanat, M. I. Kabir, T. A. Chowdhury, *The Pharma Innovation*. 1(4), 76-82 (2015)
10. K. M. Kamel, O. M. Abd El-Raouf, S. A. Metwally, H. A. Abd El-Latif, M. E. El-sayed, *Journal of biochemical and molecular toxicology*., **28(7),** 312-9 (2014)
11. S. Chandra, P. Chatterjee, P. Dey, S. Bhattacharya, *Asian Pacific Journal of Tropical Biomedicine*., **2(1),** S178-80 (2012).
12. Grande, F., Rizzuti, B., Occhiuzzi, M.A., Ioele, G., Casacchia, T., Gelmini, F., Guzzi, R., Garofalo, A. and Statti, G., 2018. Identification by molecular docking of homoisoflavones from Leopoldia comosa as ligands of estrogen receptors. *Molecules*, *23*(4), p.894.

Paper 74

SYNTHESIS, STRUCTURAL AND MAGNETIC CHARACTERIZATION OF Mg-Ni-Zn NANOFERRITE SYNTHESIZED BY USING SOL-GEL METHOD

P.R. Babar[1], D.H. Bobade[2] Sohail Bagwan [3]

[1]Ph.D. Research Scholar, Shri JJT University, Jhunjhunu, Rajasthan

[2]Department of Physics, C. T. Bora College, Shirur, Dist: Pune, (Maharashtra)

[3] Department of Physics, Abeda Inamdar Senior College, Pune (Maharashtra)

Abstract: $Mg_{0.7-x}Ni_xZn_{0.3}$ (x=0.6) is a general formula for Mg-Ni-Zn spinel ferrite. MgNiZn nano ferrite material was synthesized using the sol–gel auto-combustion process. XRD, FTIR and VSM were used to characterize the MgNiZn ferrite nanoparticles that were synthesized. The saturation magnetization and coercivity values were calculated using the hysteresis loop.

Keywords: Ferrite, Morphology, Sol-gel method, MgNiZn.

1. Introduction:

Ferrites have a high resistivity and low eddy current, making them an important magnetic material. Because they have a wide frequency range, they have a wide range of applications in the electronic and telecommunications fields [1].Several techniques have been used in recent years to produce ferrites in nanocrystalline form. Because the characteristics of these nanoparticle sized ferrites differ from those of bulk ferrites, they have applications in medication delivery, MRI, hyperthermia, sensors, catalysts, and so on [2]. In terms of characteristics and ease of use, the sol-gel chemical process has provided several advantages. Sol-gel experiments on ferrite particles containing nickel and zinc have received a lot of interest. The sol-gel method is a relatively new technology that employs organic chemicals to create ferrite cores, however it currently has a high cost in its beginning ingredients [3, 4]. The current work reports on the sol-gel synthesis of Mg-Ni-Zn ferrite.

2. Materials and Method

2.1. Materials

All chemicals including high purity analytical grade magnesium nitrate hexahydrate ($Mg(NO_3)_2 \cdot 6H_2O$), zinc nitrate hexahydrate($Zn(NO_3)_2 \cdot 6H_2O$), nickel nitrate hexahydrate

($Ni(NO_3)_2 \cdot 6H_2O$), ferric nitrate nonahydrate($Fe(NO_3)_3 \cdot 9H_2O$), and citric acid were obtained from Loba Chemie and used as received.

2.2. Preparation of $MgNiZnFe_2O_4$ Nanoparticles

Citric acid was used as the fuel in the synthesis process, with a 1:3 metal nitrate-to-citric acid ratio. The pH of the solution is adjusted to 7 using an ammonia solution. The mixed solution was further stirred on a magnetic stirrer to form a gel. It transforms from gel to ash after 4-5 hours. The ferrite powders were sintered for 1 hour at 100and 300 degrees Celsius.

The general chemical reaction in the synthesis process can be represented as

$$(0.7\text{-}x)\ Mg(NO_3)_2.6H_2O + (x)\ Ni(NO_3)_2.6H_2O + (0.3)\ Zn(NO_3)_2.6H_2O + 2\ Fe(NO_3)_3.9H_2O + 3C_6H_8O_7 \rightarrow (Mg_{0.7-x}Ni_xZn_{0.3}Fe_2O_4) + 4N_2\uparrow + 18CO_2\uparrow + 36H_2O\uparrow$$

2.3 Instrumentation:

- Characterization of the produced MgNiZn ferrite nanoparticles was accomplished using a variety of methods, including XRD, and VSM. To evaluate the structural characteristics of the produced MgNiZn ferrites, X-Ray Diffraction methods **(Miniflex 600)** and **FTIR – (Model -7600)** were employed.

3. Result and Discussion

3.1 Structural Characterization:

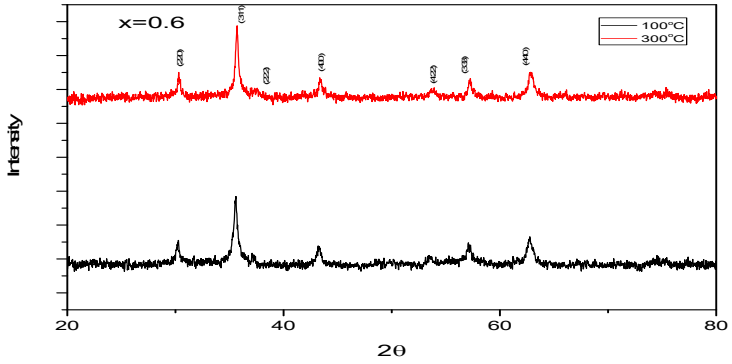

Figure-1: XRD Pattern of $Mg_{0.7-x}Ni_xZn_{0.3}$ (x=0.6) sintered at 100°C and 300°C

3.1.1 XRD Studies:

The X-ray diffraction (XRD) patterns of $Mg_{0.7-x}Ni_xZn_{0.3}$ (x=0.2) are shown in Figure-1. For all compositions and temperatures, the X-ray diffraction pattern reveals the formation of a single-phase cubic spinel structure. All of the reported XRD peaks match closely with the JCPDS patterns of cubic spinel ferrite [5].

3.1.2 FTIR ANALYSIS:

The FTIR spectroscopy is a very useful technique for deducing not only the structural investigation and redistribution of cations between spinel ferrite nanoparticles octahedral and tetrahedral sites, but also the lattice vibrational modes. All of the samples FTIR spectra show two main absorption bands at wave numbers 600 and 400 cm^{-1}, which correspond to intrinsic lattice vibrations of the ferrite skeleton for tetrahedral (A) and octahedral (B) sites, respectively [6].

3.2 VSM CHARECTERIZATION (HYSTREESSIS LOOP)

Figure-2 shows the variation of magnetic properties with sintering temperatures of the synthesized samples, it shows that the *Hc* (Coercivity) decreases and *Ms* (Magnetic saturation) increases as sintering temperature increases [5].

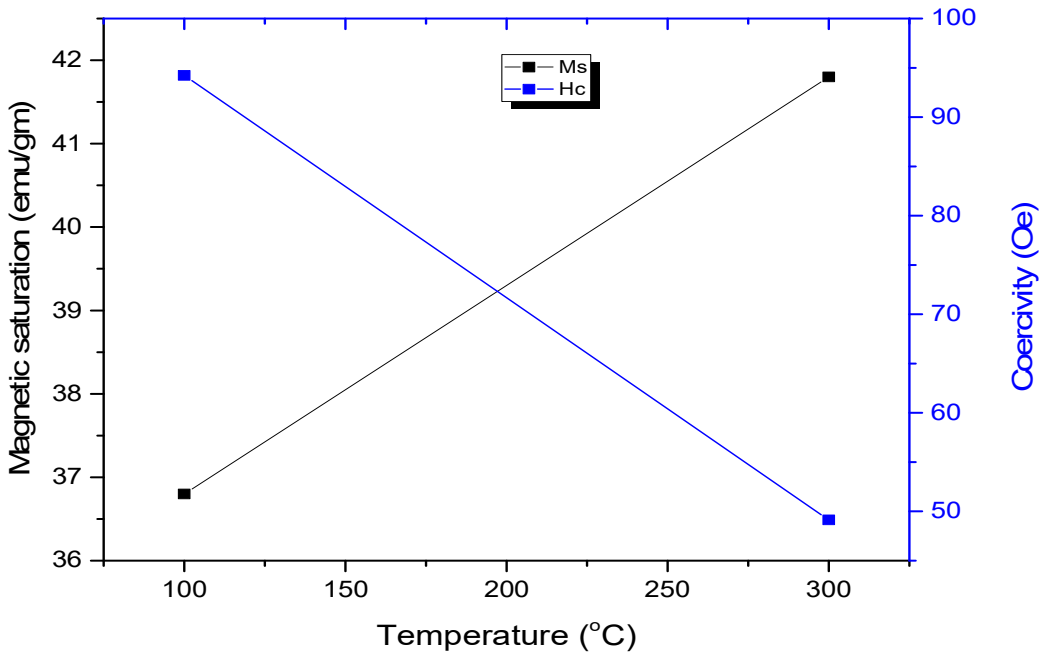

Figure 2: Variation of M_s and H_C with temperature of $Mg_{0.7-x}Ni_xZn_{0.3}$ (x=0.6) sintered at 100º and 300º Celsius.

4. Conclusion:

The $Mg_{0.7-x}Ni_xZn_{0.3}$ (x=0.6) nano ferrite system was synthesized using the sol-gel method. As the sintering temperature changes, the structural and magnetic properties of ferrites with the composition $Mg_{0.7-x}Ni_xZn_{0.3}$ (where x = 0.6) changes significantly.

5. Acknowledgement:

A researcher acknowledges DST for the availability of instruments under DST-FIST program at C. T. Bora College, Shirur (DST-FIST File No: SR/FST/COLLEGE/068/2017)

6. References:

1. V.V. Awati (2015), Synthesis and characterization of Ni0.2Cu0.1Zn0.7Fe2O4 nanoparticles by sol-gel auto combustion technique, International Research Journal, 2(5), 1-10.
2. A Thakur and M Singh (2003), Preparation and Characterization of nanosize Mn0.4Zn0.6 Fe2O4 ferrite by citrate precursor method, Ceram.Int. Volume 29, Issue 5,pp 505-511
3. S.Zahi, J.Electromagnetic Analysis and Applications, 2010, 2:56-62
4. Dyal, A., Loos, K., Noto, M., Chang, S. W., Spagnoli, C., Shafi, K. V., ... & Gross, R. A. (2003). Activity of Candida rugosa lipase immobilized on γ-Fe2O3 magnetic nanoparticles. *Journal of the American Chemical Society*, *125*(7), 1684-1685.
5. Bobade, D. H., Rathod, S. M., & Mane, M. L. (2012). Sol–gel auto-combustion synthesis, structural and enhanced magnetic properties of Ni2+ substituted nanocrystalline Mg–Zn spinel ferrite. Physica B: Condensed Matter, 407(18), 3700-3704.
6. Awati, V. V., Rathod, S. M., Mane, M. L., & Mohite, K. C. (2013). Influence of Zn 2+ doping on the structural and surface morphological properties of nanocrystalline Ni-Cu spinel ferrite. *International Nano Letters*, *3*(1), 1-8.

Paper 74

Structural and magnetic properties of nanocrystalline MgNiZn spinel ferrite synthesized via sol–gel method.

P.R. Babar[1], D.H. Bobade[2] Sohail Bagwan [3]

[1] Ph.D. Research Scholar, Shri JJT University, Jhunjhunu, Rajasthan

[2]Department of Physics, C. T. Bora College, Shirur, Dist: Pune, (Maharashtra)

[3] Department of Physics, Abeda Inamdar Senior College, Pune (Maharashtra)

Abstract:

A general formula for Mg-Ni-Zn spinel ferrite $Mg_{0.7-x}Ni_xZn_{0.3}$ (x=0.2). The sol–gel auto-combustion process was used to synthesize MgNiZn nano ferrite material. The synthesized MgNiZn ferrite nanoparticles were characterized using a variety of techniques, including XRD, SEM, FTIR and VSM The hysteresis loop was used to determine the saturation magnetization and coercivity values.

Keywords: Ferrite,Morphology, Sol-gel method, MgNiZn.

1.Introduction:

Ferrite nanoparticles, MFe_2O_4, with M being any divalent metal ion such as Mg, Mn, Ni, Co, Fe, Cu, and so on, have a wide range of uses.The maximal band gap energy of ferrites is usually around 2 eV, allowing the materials to absorb visible light effectively. Furthermore, ferrites excellent magnetic characteristics make them helpful in a variety of applications [1].When it comes to identifying the properties of ferrites, preparation approaches are crucial. The sol–gel method has a number of benefits over other methods for producing ferrite with suitable nanoarchitecture [2].The sol–gel auto-combustion method has a number of distinct advantages, including good composition control, a low-temperature process, lower production costs, and improved results [3].The sol-gel synthesis of Mg-Ni-Zn ferrite was reported in the current study.

2. Materials and Method

2.1. Materials

All chemicals including high purity analytical grade magnesium nitrate hexahydrate ($Mg(NO_3)_2 \cdot 6H_2O$), zinc nitrate hexahydrate($Zn(NO_3)_2 \cdot 6H_2O$), nickel nitrate

hexahydrate ($Ni(NO_3)_2 \cdot 6H_2O$), ferric nitrate nonahydrate($Fe(NO_3)_3 \cdot 9H_2O$), and citric acid were obtained from Loba Chemie and used as received.

2.2. Preparation of $MgNiZnFe_2O_4$ Nanoparticles

Citric acid was used as the fuel in the synthesis process, with a 1:3 metal nitrate-to-citric acid ratio.The pH of the solution is adjusted to 7 using an ammonia solution. The mixed solution was further stirred on a magnetic stirrer to form a gel. It transforms from gel to ash after 4-5 hours. The ferrite powders were sintered for 1 hour at 100, and 300 degrees Celsius.

The general chemical reaction in the synthesis process can be represented as

$$(0.7\text{-}x)\ Mg\ (NO_3)_2.6H_2O + (x)\ Ni\ (NO_3)_2.6H_2O + (0.3)\ Zn\ (NO_3)_2.6H_2O + 2\ Fe\ (NO_3)_3.9H_2O + 3C_6H_8O_7 \rightarrow (Mg_{0.7-x}Ni_xZn_{0.3}Fe_2O_4) + 4N_2\uparrow + 18CO_2\uparrow + 36H_2O\uparrow$$

2.3 Instrumentation:

A number of techniques were used to characterize the synthesized MgNiZn ferrite nanoparticles, including XRD, SEM, FTIR, and VSM, Scanning electron microscopy was used to investigate the morphological properties**(Model JSM-6360)** and **(JEOL JSM-IT 200).**X-Ray Diffraction techniques **(Miniflex 600) and** FTIR **– (Model -7600)**were used to characterize the structural properties of the synthesized MgNiZn ferrites.

3. Result and Discussion

3.1 Structural Characterization:

3.1.1 XRD Studies:

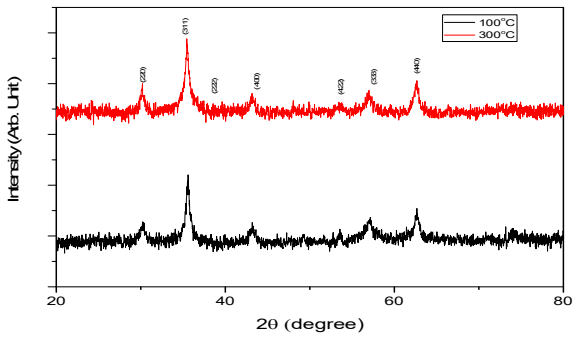

Figure-1: XRD Pattern of $Mg_{0.7-x}Ni_xZn_{0.3}$ (x=0.2)

The X-ray diffraction (XRD) patterns of $Mg_{0.7-x}Ni_xZn_{0.3}$ (x=0.2) are shown in Figure-1.For all compositions and temperatures, the X-ray diffraction pattern reveals the formation of a single-phase cubic spinel structure. All of the reported XRD peaks match

closely with the JCPDS patterns of cubic spinel ferrite[4]. The formula for calculating lattice constants is given below.

$a = d_{hkl} \times \sqrt{h^2 + k^2 + l^2}$ the miller indices are denoted as *(h k l).*

The formula used to calculate each sample's X-Ray densities is

$D_x = \frac{8M}{Na^3}$, where M denotes the sample's molecular weight, N denotes Avogadro's number, and a denotes the lattice constants.The ionic radii on the tetrahedral A and octahedral B sites are calculated using the following formulas.

$R_A = (u - \frac{1}{4}).\ a.3^{\frac{1}{2}} - r(O^{2-})$,

$R_B = (\frac{5}{8} - u).\ a\ . - r(O^{2-})$,*r(O2–)* represents the oxygen ionic radii.

Using the formula below, the length of the metal oxygen bond A–O on the tetrahedral site was calculated.

$A–O = (u - \frac{1}{4}).\ a.3^{\frac{1}{2}}$ The symbol *u* represents the oxygen ion parameter.

The following equation is used to calculate the bond length B–O on the octahedral site.

$B–O = (\frac{5}{8} - u).a$, The character *u* denotes the oxygen ion parameter.The Scherrer formula was used to determine the Average Crystallite size (D) of spinel.

D = 0.9λ/βcosθ

As sintering temperatures increases lattice constants increases, X-Ray densities decreases, bond lengths increases, ionic radii increases and crystallite size increases for all the samples. [4].

3.1.2SEM Analysis

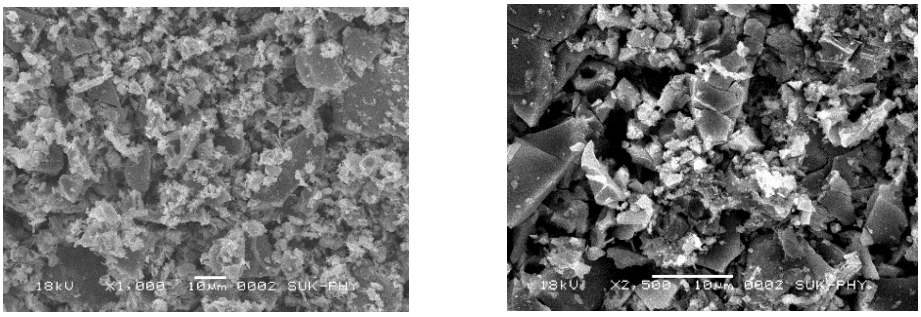

Figure 2: SEM images of $Mg_{0.7-x}Ni_xZn_{0.3}$ (x=0.2) sintered at T=100°C, 300°C, 500°

The scanning electron microscope images of the samples obtained after heat treatment at 100°C and 300°Cpresented in Figure-2.In the current investigation, all of the samples exhibit exaggerated grain growth [5].

4. VSM CHARECTERIZATION (HYSTREESSIS LOOP)

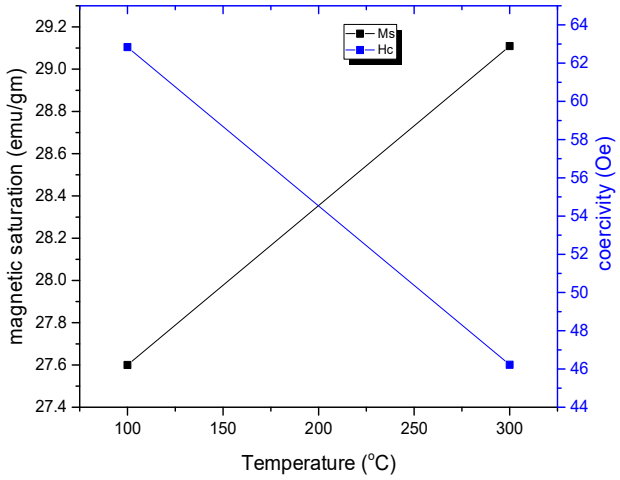

Figure-3 shows the variation of magnetic properties with temperature of the synthesized samples, it shows that the *Hc* (Coercivity) decreases and *Ms* (Magnetic saturation) increases as sintering temperature increases **[4].**

5. Conclusion:

The $Mg_{0.7-x}Ni_xZn_{0.3}$ (x=0.2) nano ferrite system was synthesized using the sol-gel method. As the sintering temperature changes, the structural, and magnetic properties of ferrites with the composition $Mg_{0.7-x}Ni_xZn_{0.3}$ (where x = 0.2) changes significantly.

6. Acknowledgement:

A researcher acknowledges DST for the availability of instruments under DST-FIST program at C. T. Bora College, Shirur (DST-FIST File No: SR/FST/COLLEGE/068/2017)

7. References:

1. Nguyen, L. T., Nguyen, L. T., Manh, N. C., Quoc, D. N., Quang, H. N., Nguyen, H. T., ... & Bach, L. G. (2019). A facile synthesis, characterization, and photocatalytic activity of magnesium ferrite nanoparticles via the solution combustion method. *Journal of Chemistry*, *2019*.
2. Shirsath, S. E., Wang, D., Jadhav, S. S., Mane, M. L., & Li, S. (2018). Ferrites obtained by sol-gel method. In Handbook of sol-gel science and technology (pp. 695-735). Springer Cham.
3. Awati, V. V., Rathod, S. M., Mane, M. L., & Mohite, K. C. (2013). Influence of Zn 2+ doping on the structural and surface morphological properties of nanocrystalline Ni-Cu spinel ferrite. *International Nano Letters*, *3*(1), 1-8.
4. Bobade, D. H., Rathod, S. M., & Mane, M. L. (2012). Sol–gel auto-combustion synthesis, structural and enhanced magnetic properties of Ni2+ substituted

nanocrystalline Mg–Zn spinel ferrite. *Physica B: Condensed Matter*, *407*(18), 3700-3704.

5. Bakale, P., Guggari, P., Keste, A., Pujar, A. S., Mathad, S. N., Hiremath, C. S., ... & Pujar, R. B. Synthesis, Structural and Mechanical Properties of Ni1-xCdxFe2O4 ferrites (X= 0.1, 0.2, 0.3, and 0.4). *combustion*, *20*, 21.